Journal of Hazardous Materials B109 (2004) 113–139

Journal of Hazardous Materials

www.elsevier.com/locate/jhazmat

Catalytic combustion of volatile organic compounds

K. Everaert [a,*], J. Baeyens [b]

[a] *Energy CA n.v., Kunstlaan 1 b3, B-1210 Brussel, Belgium*
[b] *Department of Bio-engineering, University of Antwerp, 171 Groenenborgerlaan, B-2020 Antwerp, Belgium*

Received 12 September 2003; received in revised form 1 March 2004; accepted 10 March 2004

Abstract

Despite the success of adsorption and thermal incineration of (C)VOC emissions, there is still a need for research on techniques which are both economically more favorable and actually destroy the pollutants rather than merely remove them for recycling elsewhere in the biosphere. The catalytic destruction of (C)VOC to CO_2, H_2O and HCl/Cl_2 appears very promising in this context and is the subject of the present paper.

The experiments mainly investigate the catalytic combustion of eight target compounds, all of which are commonly encountered in (C)VOC emissions and/or act as precursors for the formation of PCDD/F.

Available literature on the different catalysts active in the oxidation of (C)VOC is reviewed and the transition metal oxide complex V_2O_5–WO_3/TiO_2 appears most suitable for the current application. Different reactor geometries (e.g. fixed pellet beds, honeycombs, etc.) are also described. In this research a novel catalyst type is introduced, consisting of a V_2O_5–WO_3/TiO_2 coated metal fiber fleece.

The conversion of (C)VOC by thermo-catalytic reactions is governed by both reaction kinetics and reaction equilibrium. Full conversion of all investigated VOC to CO_2, Cl_2, HCl and H_2O is thermodynamically feasible within the range of experimental conditions used in this work (260–340 °C, feed concentrations 30–60 ppm).

A first-order rate equation is proposed for the (C)VOC oxidation reactions. The apparent rate constant is a combination of reaction kinetics and mass transfer effects.

The oxidation efficiencies were measured with various (C)VOC in the temperature range of 260–340 °C. Literature data for oxidation reactions in fixed beds and honeycomb reactors are included in the assessment.

Mass transfer resistances are calculated and are generally negligible for fleece reactors and fixed pellet beds, but can be of importance for honeycomb monoliths.

The experimental investigations demonstrate: (i) that the conversion of the hydrocarbons is independent of the oxygen concentration, corresponding to a zero-order dependency of the reaction rate; (ii) that the conversion of the hydrocarbons is a first-order reaction in the (C)VOC; (iii) that the oxidation of the (C)VOC proceeds to a higher extent with increasing temperature, with multiple chlorine substitution enhancing the reactivity; (iv) that the reaction rate constant follows an Arrhenius dependency.

The reaction rate constant k_r (s^{-1}) and the activation energy E (kJ/mol) are determined from the experimental results. The activation energy is related to the characteristics of the (C)VOC under scrutiny and correlated in terms of the molecular weight.

The k_r-values are system-dependent and hence limited in design application to the specific VOC-catalyst combination being studied. To achieve system-independency, k_r-values are transformed into an alternative kinetic constant K ($m^3/(m^2\,u)$) expressed per unit of catalyst surface and thus independent of the amount of catalyst present in the reactor. Largely different experimental data can be fitted in terms of this approach. Results are thereafter used to define the Arrhenius pre-exponential factor A^*, itself expressed in terms of the activation entropy.

Destruction efficiencies for any given reactor set-up can be predicted from E- and A^*-correlations. The excellent comparison of predicted and measured destruction efficiencies for a group of chlorinated aromatics stresses the validity of the design approach.

Abbreviations: BET, Brunauer–Emmett–Teller method for determination of surface area; CVOC, chlorinated volatile organic compounds; DClPh, dichlorophenol; GC, gas chromatography; HpCDD/F, heptachlorinated dibenzo-*p*-dioxin and dibenzofuran, respectively; HxCB, hexachlorobenzene; HxCDD/F, hexachlorinated dibenzo-*p*-dioxin and dibenzofuran, respectively; MSWI, municipal solid waste incinerator; OCDD/F, octachlorinated dibenzo-*p*-dioxin and dibenzofuran, respectively; PCB, polychlorinated biphenyls; PCBz, polychlorinated benzenes; PCDD/F, polychlorinated dibenzo-*p*-dioxins and dibenzofuran, respectively; PCPh, polychlorinated phenols; PeCB, pentachlorinated benzene; PeCDD/F, pentachlorinated dibenzo-*p*-dioxin and dibenzofuran, respectively; PeClPh, pentachlorophenol; SCR, selective catalytic reduction; TCDD/F, tetrachlorinated dibenzo-*p*-dioxin and dibenzofuran, respectively; TeCB, tetrachlorobenzene; TeClPh, tetrachlorophenol; TriCB, trichlorobenzene; TriClPh, trichlorophenol; $VO(acac)_2$, vanadyl acetylacetonate; VOC, volatile organic compounds

* Corresponding author. Tel.: +32-53-710-500; fax: +32-53-710-460.
E-mail address: kim.everaert@energy-ca.be (K. Everaert).

doi:10.1016/j.jhazmat.2004.03.019

Since laboratory-scale experiments using PCDD/F are impossible, pilot and full-scale tests of PCDD/F oxidation undertaken in Flemish MSWIs and obtained from literature are reported. From the data it is clear that: (i) destruction efficiencies are normally excellent; (ii) the efficiencies increase with increasing operating temperature; (iii) the higher degree of chlorination does not markedly affect the destruction efficiency.

Finally, all experimental findings are used in design recommendations for the catalytic oxidation of (C)VOC and PCDD/F. Predicted values of the acceptable space velocity correspond with the cited industrial values, thus stressing the validity of the design strategy and equations developed in the present paper.

Keywords: Experimental VOC oxidation; Fleece reactor; Activation energy; Reaction rate; Design

1. Introduction

Among the different techniques that can be applied to control the emissions of (C)VOC and PCDD/F, adsorption on activated carbon and thermal oxidation appeared to be the most appropriate abatement methods [1]. At present, the principal technology is adsorption on activated carbon [2], which however transfers the environmental burden from the gas to a solid phase, to be disposed off. Direct combustion has been the conventional incineration treatment for (C)VOCs, but temperatures exceeding 800–1200 °C are required to achieve complete destruction. This results in high operating costs. Incomplete combustion can give rise to a variety of by-products and insufficient control of the cooling trajectory causes the formation of PCDD/F in the flue gas [3,4]. Nitrogen oxides are also exceedingly formed in these high temperature combustion processes.

There is therefore a need for research on techniques which are both economically feasible (low energy consumption) and actually destroy the pollutants rather than merely remove them for recycling elsewhere in the biosphere. The catalytic destruction of (C)VOC to CO_2, H_2O and HCl/Cl_2 appears very promising in this context and is the subject of the present paper.

The potential of catalytic oxidation will be investigated through experiments with VOC and CVOC. These compounds are not only encountered frequently in industrial applications, but are also used in this research to simulate the behavior of PCDD/F towards catalytic destruction. Laboratory experiments with PCDD/F are impossible since the compounds are not available as commercial chemicals and would moreover be highly hazardous due to the toxicity of PCDD/F. The paper will however discuss pilot plant PCDD/F-results obtained at the MSWI of Roeselare (Belgium) and review large scale MSWI data.

Target pollutants such as mono and dichlorobenzene or chlorophenols are structurally related to PCDD/F and are often cited as precursors in the formation of these polyaromatic compounds [5]. These and other (C)VOC will be used in the experimental work.

2. Literature survey on catalytic (C)VOC oxidation processes

There have been a number of reports and patents on catalytic processes for the oxidation of CVOC [6–8], mostly related to the development of catalysts based on noble metals or transition metal oxides.

Noble metal catalysts are claimed to be highly effective, but their high cost and poor stability, especially in the presence of Cl_2 and HCl (produced when oxidizing CVOC) have limited their development [9]. A literature summary for (C)VOC oxidation over noble metal catalysts and (non-vanadia) transition metal oxides is given in reference [10].

Supported transition metal oxides of chromium, manganese, nickel, copper and cobalt [11–13] and other acidic oxide materials such as zeolites and TiO_2/SiO_2 [14] have been extensively studied, but generally they have low activity and are often subject to deactivation when used for CVOC oxidation. A catalyst based on oxides of copper and manganese supported on sodium carbonate (to capture the halogens formed) has been reported [15]. Chromium trioxide supported on porous carbon is also very active [16], but the high toxicity of chromium causes serious disposal problems with this system.

Finally, the V_2O_5–WO_3/TiO_2 catalyst has been recognized as combining a high activity and selectivity together with a strong stability in the Cl_2–HCl environment. The presence of the tungsten oxide prohibits catalyst poisoning by sulfur dioxide [17]. This type of catalyst is moreover considered state-of-the-art for the selective catalytic reduction (SCR) of NO_x emissions by NH_3, thus making the combined removal of NO_x and CVOCs possible, which obviously enhances the economic advantages of the system and makes the technique especially useful for the treatment of flue gases from, e.g. industrial or municipal waste incinerators.

A detailed review of published research concerning (C)VOC destruction using vanadia catalysts is given in Appendix A. Although the catalysts vary considerably in composition and reactor type, almost complete (C)VOC destruction can be achieved at sufficiently high temperature and residence time.

Nomenclature

A	pre-exponential factor (s^{-1})
A_m	geometric catalyst surface (m^2)
A^*	system-independent pre-exponential factor ($m^3/(m^2\,h)$)
AP	catalyst surface per unit reactor volume (m^2/m^3)
AV	area velocity = gas flow rate per unit of catalyst surface ($m^3/(m^2\,h)$)
C_{O_2}	bulk concentration of oxygen (mol/m^3)
C_{HC}	bulk concentration of the hydrocarbon (mol/m^3)
$C_{s,HC}$	concentration of hydrocarbon at the catalyst surface (mol/m^3)
C_{s,O_2}	concentration of oxygen at the catalyst surface (mol/m^3)
d	thickness of the filter cake or fleece (m)
d_p	particle diameter (m)
d_0	characteristic dimension of the catalyst geometry (m)
D_e	effective diffusivity of hydrocarbon in catalyst material (m^2/s)
D_{HC}	diffusivity of hydrocarbon in air (m^2/s)
E	activation energy (kJ/mol)
E_b	bond energy (kJ/mol)
f_v	fractional coverage of the catalyst carrier (–)
h	Planck constant (6.6256×10^{-34} J s)
ΔH_r	reaction energy (J/mol)
k_B	Boltzmann constant (1.38×10^{-23} J/K)
k_F	Freundlich constant (mg/g)
k_m	mass transfer coefficient (m/s)
k_r	intrinsic reaction rate constant (s^{-1})
k_0	apparent reaction rate constant (s^{-1})
K	system-independent intrinsic reaction rate constant ($m^3/(m^2\,h)$)
L	length of the fibers = width of the square fleece (m)
MW	molecular weight (Da)
n, m	reaction rate exponents (–)
N_h	number of fibers stacked over the fleece height (–)
N_l	number of fibers per horizontal layer (–)
N_T	total number of fibers in the fleece (–)
Q	flow rate (m^3/s)
R	universal gas constant (J/(mol K))
R_{HC}	rate of reaction ($mol/(m^3\,s)$)
Re	Reynolds number (–)
Sc	Schmidt number (–)
Sh	Sherwood number (–)
SV	space velocity (s^{-1})
ΔS	activation entropy (J/(mol K))
t	residence time (s)
T	temperature (°C or K)
u	gas velocity (m/s)
V	catalyst volume (m^3)
V_m	the fiber volume (m^3)

Greek letters

δ	thickness of catalyst washcoat (m)
ε	porosity (–)
η	destruction efficiency (–)
ϕ	catalyst effectiveness factor (–)
ϕ_T	Thiele modulus (–)

Since a catalyst's activity is mostly limited to its outer surface, there is a strong economic incentive to disperse this expensive component as finely as possible on some sort of inert or moderately active support. As shown in Appendix A, titania and γ-alumina are the most commonly encountered supports for the V_2O_5 catalyst. Both materials display good dispersion properties, a high degree of porosity and are relatively easily coated with active components. Some reports also mention zirconia, silica and lanthana carriers. In general, a higher (C)VOC oxidation activity was noticed for titania supported catalysts [18], which instigated our choice for this type of support.

Catalyst systems are encountered in a large variety of designs. The catalyst can serve as its own support. This is the case in the frequently used pelleted catalysts that are mostly spherical and have diameters ranging from 2 to 5 mm. The mass transfer resistance will be important in large particles, while a significantly higher pressure drop will be experienced in a fixed bed of smaller particles. The Shell catalysts, which contain catalytic species concentrated near the particles' outer surface, are a possible remedy for this dilemma. Other important disadvantages of fixed bed catalysts are possible maldistributions resulting in non-uniform access of reactants to the catalytic surface and unfavorable local process conditions.

Alternatively, the support can be applied on the surfaces of a honeycomb-like monolithic block. The total walled area of all of these small channels provides a high specific geometric surface area, which explains the high volumetric activity of the monolith honeycomb reactor. The flow through the straight channels of the honeycomb reactor of the monolithic matrix is subject to very low pressure drops, which may be greater by two or three orders of magnitude in a packed bed with the same external geometric surface area [19].

Other possible support materials are parallel plates and fiber pads and gauzes. These types of catalysts are obtained by depositing the catalytic material onto a stainless steel net or perforated metal plate. As in the case of honeycomb matrices, the parallel plates are assembled in modules and inserted into the reactor in layers. Metal gauzes are manufactured by weaving techniques and more recently also by computer-controlled knitting. Knitted webs are less fragile than their woven counterparts and their bulky

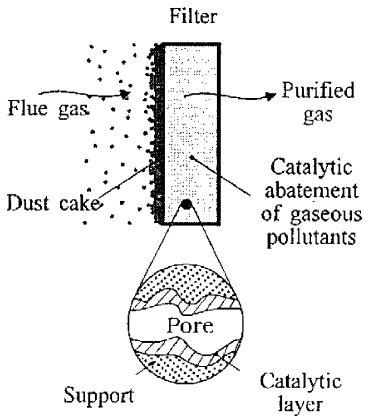

Fig. 1. Cross-sectional view of a catalytic filter [52].

three-dimensional structure gives them additional surface area. Wire life is longer than for traditional gauzes and mechanical damage leading to catalyst loss is reduced. Moreover, it appears that gas flow through knitted gauzes leads to less solid particles being trapped on the surface.

Catalytic combustion processes mostly use honeycomb or fixed bed reactors. This work presents a novel catalytic concept where the catalyst is deposited on the fibers of a sintered metal fleece. This system has the advantage of high mass transfer efficiency between the gas stream and the catalyst, with low pressure drop, and if required combining the catalytic destruction of (C)VOCs with particulate removal (dedusting efficiency > 99.9% pure) [20], thus avoiding pore clogging and/or catalyst poisoning by fly-ash components (Fig. 1). Since (C)VOCs are known to adsorb readily onto dust particles (e.g. adsorption of PCDD/F on fly ash in MSWIs), efficient dedusting of the gas stream can be necessary to meet the required emission standards. An equivalent Teflon support, but with embedded catalyst, the Goretex Remedia^{TM} filter, has also been studied.

The final choice between the different available catalyst systems depends on the application and personal preference.

3. Theoretical treatment of catalytic combustion

3.1. Chemical equilibrium for catalytic oxidation reactions

The conversion of CVOCs by thermo-catalytic reactions is governed by both reaction kinetics and reaction equilibrium. Prior to assessing the kinetics of the oxidation reactions, it is important to study the complex equilibria of the destruction reactions within the further applied temperature range of 260–340 °C. These equilibria can be studied either by solving the simultaneous equilibrium expressions or minimizing the total free energy. Both approaches are presented by AspenPlus (version 10.2) and detailed in Ref. [10].

The calculation by the simultaneous equilibrium method is hereafter illustrated for the oxidation of trichloroethylene. The oxidation of trichloroethylene can proceed through different pathways. The following reaction scheme can be proposed [21]:

(1) $C_2HCl_3 + O_2 \rightarrow 2CO + HCl + Cl_2$
(2) $CO + \frac{1}{2}O_2 \rightarrow CO_2$
(3) $C_2HCl_3 + 2O_2 \rightarrow 2CO_2 + HCl + Cl_2$
(4) $C_2HCl_3 + Cl_2 \rightarrow C_2Cl_4 + HCl$
(5) $C_2Cl_4 + 2O_2 \rightarrow 2CO_2 + 2Cl_2$
(6) $2HCl + \frac{1}{2}O_2 \rightarrow H_2O + Cl_2$

Reaction (6) is the well-known Deacon reaction which occurs since water, oxygen and chlorine are present in the reaction environment. Reactions (1) and (2), and (4) and (5) are clearly not independent. The overall equilibrium is hence determined by reactions (2) and (4).

The equilibrium was calculated in the temperature range of 200–400 °C for a reaction environment with 21 mol% O_2 and a pollutant feed concentration of 5 mol% trichloroethylene. The values of the equilibrium constants were in the order of 10^{20} for reactions (2)–(4), and approximately 65 for reaction (5). It is thus theoretically possible to fully oxidize trichloroethylene to CO_2, Cl_2, HCl and H_2O.

The equilibrium calculations were validated in the experimental investigations as detailed further in the paper.

For other groups of experimentally investigated VOCs (alcohols, aromatics, chlorinated aromatics), representative compounds were examined in a similar way. Results of calculations for methanol, benzene, monochlorobenzene, 1,2-dichlorobenzene and toluene [10] confirm that full conversion of all investigated VOCs to CO_2, Cl_2, HCl and H_2O is thermodynamically feasible within the range of experimental conditions used in this work (260–340 °C, feed concentrations 30–60 ppm). For some compounds, e.g. monochlorobenzene, a small fraction will still be present at equilibrium when starting from an extremely high inlet concentration (e.g. 4.8 mol%), thus implying that a total removal of this compound from the inlet stream is impossible no matter how long a reaction time is used. The oxygen depletion is also clearly illustrated in the respective amounts of HCl and Cl_2 being present in the reaction products (Deacon reaction).

3.2. Catalytic combustion kinetics

3.2.1. Generalities

Catalytic combustion involves the use of a solid catalyst. The role of the catalyst is to provide an alternative reaction pathway between reactants and products by lowering the activation energy of the reaction. For combustion reactions, the energy of the products is always lower than the energy of the reactants. The reaction is hence accompanied by a significant release of thermal energy. This also means that the activation energy for the reverse reaction is very much higher than for the forward reaction, which explains the high equilibrium yield for these reactions.

The catalyst activity only influences the reaction kinetics. Reactions that are thermodynamically impossible, cannot take place even in the presence of a catalyst.

A rise in temperature also increases the reaction rate since the average level of energy of the molecules also increases and a higher fraction will possess the necessary activation energy for reaction. The operational costs will however increase and unwanted by-products may be formed at high temperatures.

The use of a catalyst offers an additional advantage, i.e. its selectivity, as it often suppresses the formation of reaction by-products. This results in an optimal use of the reactants and in a reduction of the possibly generated waste stream.

3.3. Reaction rate equation

Literature involving kinetic rate expressions for the oxidation of (C)VOCs is very limited. The reaction mechanism is believed to involve either a reaction between adsorbed oxygen and adsorbed reactant molecules (Langmuir–Hinshelwood mechanism) or a reaction between chemisorbed oxygen and the gas-phase reactant (Eley–Rideal mechanism).

Both mechanisms are based on the Langmuir model [22] for the description of the adsorption steps and the surface reaction is considered to be the rate determining step.

The rate equation can be expressed in terms of catalyst volume and substance concentration:

$$-R_{HC} = k_0 C_{HC}^n C_{O_2}^m = \phi k_r C_{s,HC}^n C_{s,O_2}^m \quad (1)$$

with R_{HC} being the rate of reaction of the hydrocarbon, defined in mol/(m^3 s), k_0 the apparent rate constant given in s^{-1}, C_{HC} the bulk concentration of the hydrocarbon (mol/m^3), C_{O_2} the bulk concentration of oxygen (mol/m^3), ϕ the effectiveness factor (–), k_r the reaction rate constant (s^{-1}), $C_{s,HC}$ the concentration of hydrocarbon at the catalyst surface (mol/m^3), C_{s,O_2} the concentration of oxygen at the catalyst surface (mol/m^3) and n, m the rate exponents of the reaction ($n = 1$ and $m = 0$, see Section 5.1).

Experimental results will prove that there is no substantial internal diffusion resistance in the wash coat of the fleece ($\phi = 1$) and that the catalytic combustion of hydrocarbons is of the zero-order with respect of oxygen. The equation can hence be written as a power law expression of first order with respect of the bulk concentration of the hydrocarbon:

$$R_{HC} = \frac{dC_{HC}}{dt} = -\frac{k_r C_{HC}}{1 + (k_r V / k_m A)} \quad (2)$$

with V/A = catalyst volume (m^3)/geometric catalyst surface (m^2) = d = thickness of catalyst washcoat, k_m the mass transfer coefficient of HC (m/s).

After integration and combination with Eq. (1), Eq. (2) results in:

$$\frac{C_{HC}}{C_{HC,0}} = \exp(-k_0 t) \quad (3)$$

or

$$\ln(1 - \eta) = -k_0 t \quad (4)$$

with $C_{HC,0}$ being the initial bulk concentration of the hydrocarbon (mol/m^3) and $\eta = C_{HC,0} - C_{HC}/C_{HC,0}$ the destruction efficiency of the reaction (dimensionless).

The apparent rate constant k_0 is a combination of reaction kinetics and mass transfer rate:

$$\frac{1}{k_0} = \frac{\delta}{k_m} + \frac{1}{k_r} \quad (5)$$

The effect of catalytic reactor geometry on the mass transfer resistance and apparent rate constant will be illustrated in the experimental discussion.

4. Experimental

4.1. Laboratory investigations

4.1.1. Target (C)VOC

The experiments were conducted mainly to study the catalytic combustion of eight target compounds (Fig. 2): benzene (Bz), monochlorobenzene (MCB), 1.2-dichlorobenzene (DCB), 2-chlorophenol (MClPh), trichloroethylene (TCE), 1,1,1-trichloroethane (TCA), toluene (TOL) and methylcyclohexane (MCH). All target compounds are commonly encountered in (C)VOC emissions and some of them are suspected precursors for the formation of PCDD/F. They therefore need emission abatement and are potential candidates for catalytic combustion. As illustrated in Table 1, the compounds show structural difference and similarity, which could provide an insight into the mechanism of the catalytic oxidation.

Since the objective was to expand experimental findings to PCDD/F destruction, and since laboratory experiments with single/mixed PCDD/F congeners are impossible (commercially not available and extremely toxic), the target (C)VOC selection was also determined by other factors:

- Polychlorinated benzenes, chlorinated phenols and PCB are formed alongside PCDD/F and their concentrations

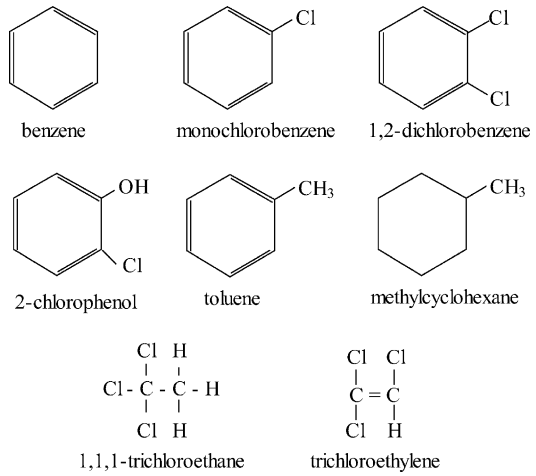

Fig. 2. Chemical structure of the target compounds.

Table 1
Objectives of the experiments

Comparison of compounds	Examined effect on catalytic activity
Benzene, MCB and DCB	Degree of chlorine substitution
DCB and MClPh	Chlorine vs. hydroxyl substitution
TCE and TCA	Chlorinated, unsaturated vs. saturated molecule
Toluene and methylcyclohexane	Non-chlorinated, unsaturated vs. saturated molecule

are proportional to the PCDD/F concentration [10]. They can be used as marker components, but must also be eliminated from the emitted gases.

- Chlorophenols and other aromatic and even aliphatic compounds are recognized as precursors to PCDD/F formation. Their abatement is hence an important preventive measure to PCDD/F formation.
- By investigating the influence of the number of chlorine substituents, of the presence of hydroxylgroups, of the saturated versus unsaturated and of the cyclic versus the aliphatic nature of the molecules, underlying combustion mechanisms might be derived which can be extrapolated to PCB and PCDD/F. This strategy of extrapolation will be used in the discussion of the experiments, where predicted PCDD/F destruction efficiencies and literature data will be assessed.

4.1.2. Selection of the catalyst

As reviewed in Section 2, the V_2O_5–WO_3/TiO_2 catalyst has been recognized as combining high activity and selectivity together with a strong stability in Cl_2–HCl environments. The catalyst system used in the investigations contains a well-known concentration of V_2O_5, WO_3 and TiO_2 deposited on a sintered metal fleece.

4.1.3. Preparation of the catalyst and coating of the sintered metal fleece support

Three different coating techniques were developed in collaboration with the Laboratory of Adsorption and Catalysis of the University of Antwerp (Belgium), i.e. dipping, spraying and chemical vapor deposition (CVD). In order to remove any surface contamination and guarantee a good adhesion of the oxides on the metal fleece surface, the virgin metal fleece was precalcined overnight in ambient air from room temperature to 450 °C at a heating rate of 1 °C/min. The mixed titanium–tungsten oxide coating solution was prepared by dissolving titanium (IV) isopropoxide and tungsten (VI) chloride in isopropanol with a complexing agent. Some distilled water and nitric acid, dissolved in isopropanol, were slowly added to the Ti–W-solution under vigorous stirring. The components were added in such ratios that the required molar gel composition was obtained. Gelation occurred within 8 h and the resulting gel was aged for 16 h. Vanadyl acetylacetonate ($VO(acac)_2$) was dissolved in the resulting Ti–W-gel. The entire mixture was aged for another 24 h. All solutions were prepared at least 24 h in advance of the coating process.

Although the CVD process is the most efficient coating technique, it is also the most expensive one. Industrial application for large filter candles is tedious since the elements have to be placed in a sealed vessel of appropriate dimensions. The method was therefore abandoned.

Dip coating requires numerous successive cycles of dipping and drying. It is a very time-consuming method and not used in the research.

In spray coating, the precalcined fleece is mounted onto a spinning plate and V–Ti–W solution is pressure sprayed using N_2. After several hours of spraying, followed by ambient drying, the metal fleece is calcined at 450 °C during 24 h. This application technique uses a considerably reduced quantity of sol–gel in comparison with a dip process. Spray coating is satisfactory since the fiber-web has no internal pores and only the external surfaces need coating. It is a widely applicable method due to its adaptability to almost any condition, shape or size of the object. The wastage of catalyst solution due to overspray can be limited by using both a constant spinning speed and solution flow rate; the spinning rate was moreover adjusted to the viscosity of the solution.

4.1.4. Catalytic fleeces used in the research

4.1.4.1. Sintered metal fleeces (Bekaert). Sintered metal fleece carriers were obtained from Bekaert Advanced Filtration (Belgium) and spraycoated with the mixed catalyst. The metal fleeces used have thickness of 1000 μm and differ in fiber diameter (2 or 4 μm). The absolute density of the fibers is 8320 kg/m^3. The medium can be approximated by the square mesh of Fig. 3. Given the geometry of the fleece, the following characteristics are important:

- m: weight of the fleece,
- d: total thickness of the fleece,
- L: length of the fibers, is supposed to be equal to the width of the square fleece,
- d_f: fiber diameter,

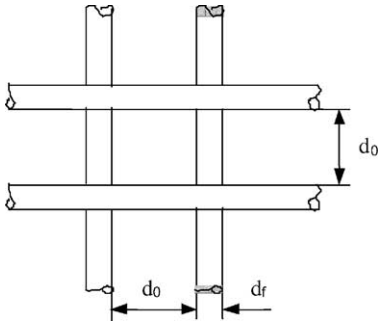

Fig. 3. Schematic (idealized) representation of a unit-cell of the fiber fleece.

Table 2
Characteristics of the tested metal fleeces

Fleece thickness, d (μm)	1000	1000
Fiber diameter, d_f (μm)	4	2
Width, L (m)	0.090	0.090
Weight, m (g)	10.1	9.6
Porosity, ε (–)	0.85	0.86
N_h	250	500
N_T	1074296	4297183
N_l	4297	8594
d_0 (μm)	8.5	16.9
A_m (m^2)	1.22	2.43
V_m (m^3)	1.22×10^{-6}	1.22×10^{-6}
BET (m^2/g)	25	30
wt.% V_2O_5	3.2	3.5
wt.% TiO_2	2.7	2
wt.% WO_3	1	1
Washcoat thickness, δ (μm)	0.15	0.07
Coating method	Spray	Spray

- ε: porosity of the $1 - m/dL^2 8320$,
- N_h: number of fibers stacked over the fleece height $= d/d_f$,
- N_T: total number of fibers in the fleece $= (1-\varepsilon)L^2 d/L(\pi d_f^2/4)$
- N_l: number of fibers per horizontal layer $= N_T/N_h$,
- d_0: average distance between two fibers in the layer $= L - N_h d_f/N_h$,
- A_m: geometric surface area of the catalyst $= N_T \pi d_f L$,
- V_m: fiber volume $= N_T(\pi d_f^2/4)L$,
- the BET-surface area, determined by N_2 adsorption–desorption at −196 °C in a Quantachrome Autosorb Automated Gas Sorption System (Micropore version 2.48),
- the fractional composition of the catalyst, determined by ICP-MS after dissolving the fleece, and
- the thickness of the catalyst washcoat on the fleece fibers, δ, calculated from the catalyst composition, the weight of the fleece and the density of V_2O_5, TiO_2 and WO_3 (respectively, 3.36, 3.84 and 7.16 g/cm^3).

Numerical values of these characteristics are summarized in Table 2.

4.1.4.2. Goretex Remedia® catalytic fleeces. As previously described in detail [23], this catalytic filter system is manufactured by W.L. Gore & Associates, Inc. (Gore) and sold under the trade name REMEDIA D/F Catalytic Filter System®. The catalyst is incorporated into a dispersion of PTFE. After drying, the dispersion is extruded into a thin tape. The tape is stretched and chopped into short staple fibers. The staple fibers are needle-punched into a PTFE scrim to form a coherent felt. In the last step of this process, a microporous membrane is laminated to the felt forming the final product, the Goretex REMEDIA® catalytically active filter.

The fleeces tested in this research had a thickness 980 μm, a cross-sectional area of 0.09 m × 0.09 m and a porosity of 0.6. The fleeces had an average weight of 8.3 g and contained 7.5 wt.% V_2O_5 for a BET of 85 m^2/g.

4.1.5. Experimental set-up and procedure

Oxidation reactions were carried out in the experimental set-up of Fig. 4. The outlet and inlet sections were stuffed with metal wool to ensure uniform distribution of air and VOC. A residence time distribution measurement proved that no dead area was present. The wool of the outlet section was mixed with porous $Ca(OH)_2$-pellets to capture the possible reaction byproducts HCl and Cl_2.

The feed stream was preheated to a given temperature at a given feed rate (up to 1 N m^3/h). The flow rate of VOC was set by altering the speed of the piston-pump discharge. A fraction of the influent and effluent air stream was analyzed by a Shimadzu gas chromatograph (type GC-14A) equipped with FID-detector. CO and CO_2 were monitored separately using a Testotherm monitor. Samples were also taken on activated carbon probes that were subsequently desorbed with CS_2 and analyzed by GC-MS. The concentrations of the injected and residual (C)VOC as well as other chlorinated and non-chlorinated by-products could hence be determined.

4.2. Industrial investigations

As stated before, laboratory experiments using PCDD/F are hardly possible as these components are not commer-

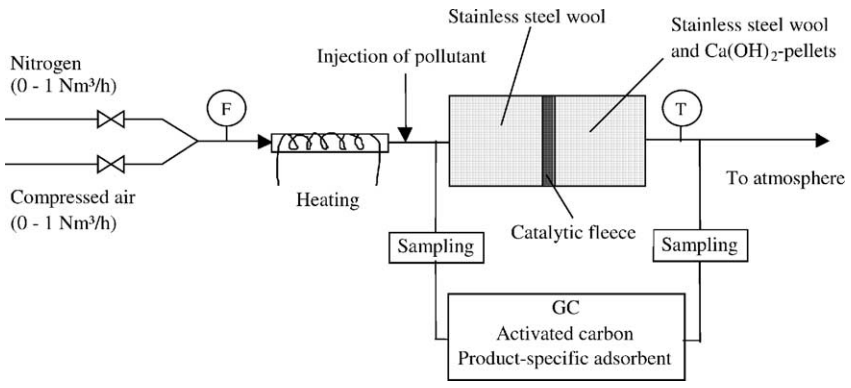

Fig. 4. Experimental set-up.

cially available. Experiments are therefore commonly carried out either on a side-stream of an existing MSWI-plant after the boiler and primary dedusting in the case of pilot studies, or in a full-scale catalytic filter.

The former approach was used by the authors at the MSWI of Roeselare (IVRO) and various researchers quoted in the literature. Data from full-scale operation were collected by the authors in the Flemish MWSIs using catalytic filters and were also taken from literature.

It should moreover be remembered that some data are rather inaccurate due to the concentration of some congeners below the detection limit, but accounted for at this limit concentration and hence resulting in too low a destruction efficiency.

At the MSWI of IVRO (Roeselare), measurements were carried out on a by-pass stream (approximately 3000 N m^3/h) of the IVRO flue gas. The experimental set-up was equipped with the Goretex REMEDIA fleece.

5. Results of laboratory investigations

5.1. Preliminary observations

(i) Prior to performing decomposition reactions using the catalytic fleece, the possible effect of the virgin sintered metal fleece and associated stainless steel reactor and packing was studied at temperatures between 250 and 325 °C. The results showed no destruction effect.

(ii) As suggested by Weber et al. [23], a distinction should be made between the removal (η_r) and the destruction (η_d) efficiency, the difference being the concentration of possibly adsorbed (C)VOC on the catalyst. This phenomenon generally occurs at temperatures below 200 °C. Both efficiencies are defined as:

$$\eta_r = \frac{C_{in} - C_{out}}{C_{in}} \quad \text{and} \quad \eta_d = \frac{C_{in} - (C_{out} + C_{ads})}{C_{in}} \qquad (6)$$

Although our experiments were carried out at temperatures in excess of 250 °C, the possible effect of adsorption was studied by testing a catalytic fleece used in the reaction of TCE and toluene for adsorbed components. Parts of the fleece were extracted with CS_2 and/or *i*-propanol, and the extracts were analyzed by GC. No traces of the components were found, thus stressing the fact that adsorption is negligible in the experiments. Removal and destruction efficiencies are therefore equal and further indicated in the text as η.

(iii) The effect of the oxygen concentration was also studied. The measured outlet concentration of VOCs for varying vol.% of oxygen is given in Fig. 5. Since the outlet concentration is independent of the oxygen content of the feed gas, it is clear that the rate of reaction is of zero-order with respect to O_2 within the tested concentration range (>3 vol.% O_2).

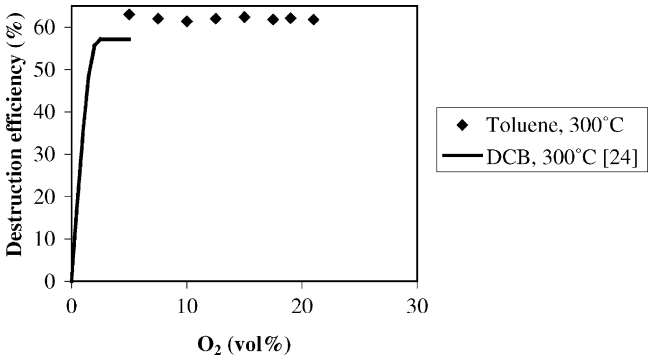

Fig. 5. Effect of the oxygen concentration in the reactor on VOC-oxidation.

Similar results have been given in literature [24], and are also included in Fig. 5. The oxygen concentration has a marked effect below 3 vol.%.

The zero-order dependency is attributed to the catalyst surface being saturated with dissociatively chemisorbed oxygen:

$$O_2 + (\,) \rightarrow (O_2) \rightarrow 2(O)$$

with ( ) and (O) representing a reduced and oxidized site, respectively. This dissociative chemisorption is followed by direct reaction of the gaseous VOC [21] with (O) and corresponds with the Eley–Rideal mechanism.

(iv) The influence of the inlet concentration of VOC was tested for varying feed concentrations of TCE and toluene at constant contact time over the fleece. Fig. 6 shows that the feed concentration does not affect the conversion, thus proving the first-order reaction for the VOCs. The same result was obtained by Krishnamoorthy et al. [24] for different concentrations of 1,2-dichlorobenzene and is also illustrated in Fig. 6.

(v) The selectivity of the catalyst was tested for TCE (see Section 3.1) and other target (C)VOC. When, e.g. using TCE, on-line GC-analysis (and GC-analysis of samples taken on active carbon probes) of the reactor outlet confirmed the absence of C_2Cl_4, while no traces of CO were detected by on-line IR analysis. The chlorine balance could not be measured since HCl and Cl_2 are immediately captured on the $Ca(OH)_2$ pellets after the

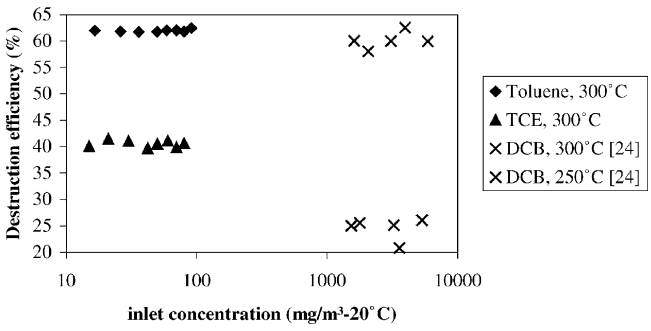

Fig. 6. Effect of the inlet concentration of VOC on oxidation.

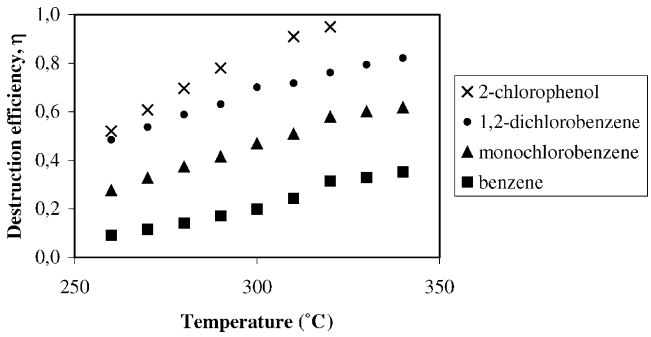

Fig. 7. Experimental destruction yields for target VOC.

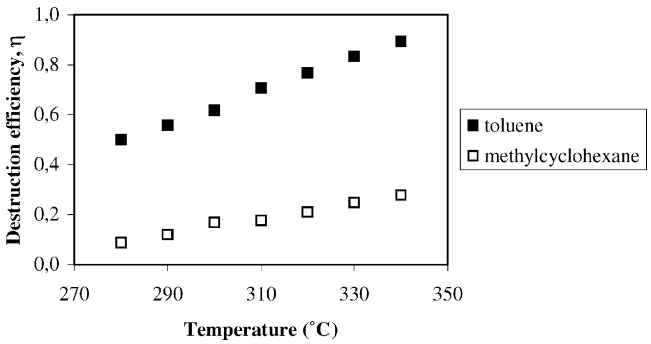

Fig. 8. Experimental destruction efficiencies for non-chlorinated compounds.

catalytic fleece. No detectable reaction products other than CO_2 and H_2O were present when testing other (C)VOC. It can therefore be concluded that the catalyst shows indeed an excellent selectivity.

5.2. Summary of experimental data

5.2.1. Benzene, monochlorobenzene, 1,2-dichlorobenzene and 2-chlorophenol

Benzene, monochlorobenzene, 1,2-dichlorobenzene and 2-chlorophenol were chosen as target components to study the effect of the chlorination degree and the presence of a hydroxylgroup on the destruction efficiency of an aromatic molecule.

The experimental results are illustrated in Fig. 7 The investigated components auto-ignite at temperatures in excess of 550 °C. Therefore, the use of the catalyst presents a reduction of at least 300 °C in comparison with the homogeneous oxidation reaction.

The oxidation rate of the benzenes appears to increase with increasing chlorination degree. This can be explained by both a reduction of activation energy (as will be shown later) and by a change in volatility and adsorption characteristics with chlorination degree [23]. The volatility of the benzenes decreases with increasing chlorination degree as can be derived from the boiling points (80 °C for benzene, 131 °C for monochlorobenzene and 180 °C for 1,2-dichlorobenzene). The higher chlorinated forms are therefore longer retained on the catalyst, thus increasing their chance of oxidation.

There are however two competing effects depending on the chlorination degree. This is illustrated by the difference in oxidation behavior between 2-chlorophenol and 1,2-chlorobenzene, compounds with comparable volatilities (boiling points are, respectively, 176 and 180 °C). The second effect to be taken into account is the electron withdrawal from the aromatic ring structure by substituents with a very negative electron affinity [25]. This explains the lower oxidation rate of 1,2-dichlorobenzene in comparison with 2-chlorophenol, since a chlorine substituent has a higher negative electron affinity (−348 kJ/mol) than a hydroxylgroup (−219 kJ/mol) [26].

The effect of the increased redox potential by chlorine substitution is however not noticed when comparing the oxidation rates of the benzene, monochlorobenzene and 1,2-dichlorobenzene because their boiling points are so far apart that the effects of volatility and adsorption are dominant.

5.2.2. TCE and toluene versus TCA and methylcyclohexane

The effect of double bonds (C=C) on the oxidation behavior of a molecule is investigated by comparison of the destruction efficiencies for trichloroethylene (TCE) and toluene on the one hand and, respectively, 1,1,1-trichloroethane (TCA) and methylcyclohexane on the other hand.

Fig. 8 demonstrates that the oxidation of toluene proceeds to a higher extent than the oxidation of its corresponding unsaturated molecule, methylcyclohexane, because the unsaturated bonds are more readily ionized or polarized [27,28].

Fig. 9 however shows the opposite behavior for the chlorinated hydrocarbons TCE and TCA, yet similar to that reported by Windawi and Wyat [29] and Gonzalez-Velasco et al. [30] for the oxidation of TCE, dichloroethane and several other CVOC over Pt and Pd catalysts.

Chlorinated alkanes are oxidized more readily than chlorinated alkenes. This can be explained by the high electronegativity of chlorine: the electronic charge of the molecules is drawn towards the chlorine atoms, which protects the molecules from oxidation. This effect is more pronounced in alkenes since the electrons in an unsaturated bond have a greater mobility.

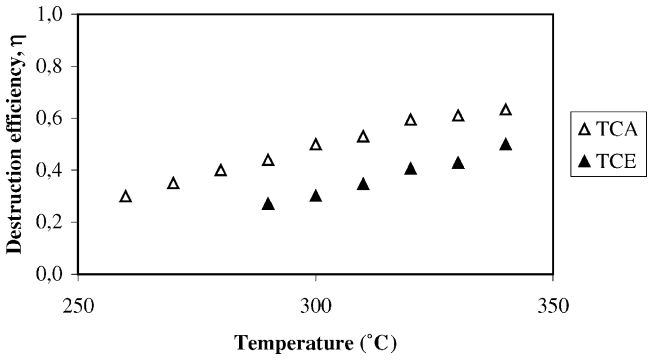

Fig. 9. Experimental destruction efficiencies of TCE and TCA.

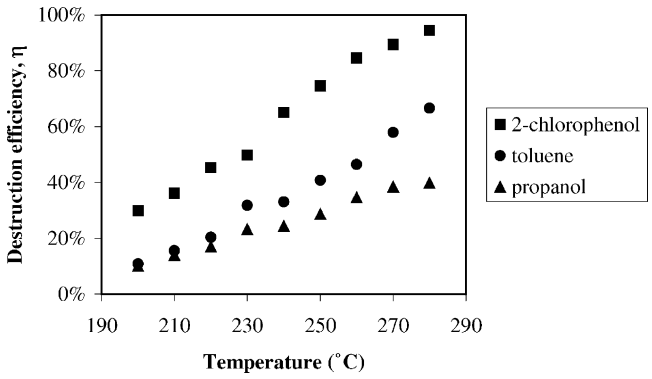

Fig. 10. Experimental destruction efficiencies for Goretex REMEDIA®.

When looking at the rather low destruction efficiencies for, e.g. TCE and methylcyclohexane, one must remember that the microreactor used in these experiments contained two fleeces, each of 1 mm thickness, and had a residence time of approximately 26 ms only. For the first-order reaction of VOC-oxidation, an exponential relationship exists between destruction efficiency and residence time. An increase in residence time will therefore significantly increase the destruction yield. A higher residence time can easily be obtained by increasing the catalytic fleece surface, e.g. by adding or using thicker fleeces. For example, the residence time in the reactor can be doubled by inserting two extra fleeces. The destruction efficiency of TCE, a compound that is known as difficult to oxidize, will then increase from 30 to 52% (300 °C, $k_0 = 13.9\,s^{-1}$). At a fourfold of the original residence time, i.e. with a fleece of 8 mm thickness, the destruction efficiency will increase to 76%.

For the experiments however, we deliberately chose to work with these low residence times because no kinetic data can be deduced when the destruction efficiencies of virtually all investigated compounds are 100%.

5.2.3. Oxidation of (C)VOC over Goretex REMEDIA® fleece

The results of the tests for several (C)VOC are illustrated in Fig. 10. Results are in line with the sintered metal fleece although the reaction appears to proceed at the same rate for slightly lower temperatures due to the very high concentration of V_2O_5.

5.3. Evaluation of the contribution of mass transfer to the measured kinetics

5.3.1. External mass transfer resistance

The reaction rate equation involves reaction kinetics and mass transfer resistance. The mass transfer coefficient, k_m, can be calculated from the Sherwood number, itself being a function of the Reynolds number:

$$k_m = \frac{Sh\, D_{HC}}{d_0} \tag{7}$$

with Sh being the Sherwood number, D_{HC} the diffusivity of the hydrocarbon in air at temperature T (°C) (m^2/s) and d_0 the characteristic dimension of the catalyst geometry (m).

To assess the mass transfer impact, its effect was calculated for the tested flow rate (Q) of 0.91 N m^3/h at an average experimental temperature (T) of 300 °C. Under these conditions, the following properties prevail:

- The residence time in each fleece is 12.9×10^{-3} s and is calculated as follows:

$$t = \frac{\varepsilon L^2 d}{Q(T + 273/273)} \tag{8}$$

  with ε being the overall voidage of the fleece (–), L the width of the square fleece (m) and d the thickness of the fleece (m).
- The experimental superficial gas velocity is 0.066 m/s ($=(Q/L^2)(T + 273/273)$), resulting in a Reynolds number in the order of 10^{-2}.
- For small values of the Reynolds number ($\ll 1$), the Sherwood number can be calculated as: $Sh \approx 0.12\,Re^{1.06}$ [31], and amounts to 1.1×10^{-3} for the 2 μm fleece and 2.2×10^{-3} for the 4 μm fleece.
- The diffusivity in air for the examined components is of the order of 2.5×10^{-5} m^2/s (Table 3) and can be calculated from [32].

As a result of the low values of Sh, D_{HC} and d_0, the value of the mass transfer coefficient k_m is of the order of 3×10^{-3} m/s for the examined components.

Given the washcoat thickness, δ, from Table 2 and having experimentally measured the apparent reaction rate constant k_0, it is now possible to determine the intrinsic reaction rate constant k_r. From the results in Table 3, it is evident that the external mass transfer resistance can be neglected and that the apparent and intrinsic reaction rate constant are equal, thus

$$\ln(1 - \eta) = -k_r t \tag{9}$$

A similar conclusion is obtained for the gas flow through the fine web of the Goretex REMEDIA® filter. The effect of the mass transfer resistance in different reactor geometries (e.g. honeycomb, fixed bed reactor) will be assessed in Section 6.2.

5.3.2. Internal mass transfer resistance

In the previous section, the pore diffusion resistance was assumed to be negligible. The effectiveness factor, ϕ, can be evaluated as a function of the Thiele modulus, ϕ_T:

$$\phi = \frac{1}{\phi_T}\left(\frac{1}{\tanh 3\phi_T} - \frac{1}{3\phi_T}\right) \tag{10}$$

Eq. (10) was derived for the case of spherical pellets and a first-order reaction. The effect of catalyst shape on the ϕ-versus-ϕ_T relationship however has been examined by several investigators [33,34] and the shape of the catalyst is not significant for a first-order reaction [35].

Table 3
Contribution of external mass transfer resistance to the apparent rate constant

	D_{HC} ($\times 10^{-5}$ m^2/s)	δ/k_m ($\times 10^{-5}$ s)	$1/k_0$ ($\times 10^{-2}$ s)	$1/k_r$ ($\times 10^{-2}$ s)	$(\delta/k_m)/(1/k_0)$ (%)
Benzene	2.81	6.02	11.6	11.6	0.05
Monochlorobenzene	2.50	6.77	4.10	4.09	0.17
1,2-Dichlorobenzene	2.28	7.40	2.15	2.14	0.34
2-Chlorophenol	2.22	7.60	1.12	1.12	0.68
TCE	2.61	6.47	7.19	7.19	0.09
TCA	2.57	6.59	3.73	3.72	0.18
Toluene	2.52	6.70	2.69	2.68	0.25
Methylcyclohexane	2.25	7.52	14.1	14.1	0.05

The Thiele modulus, ϕ_T, is calculated as

$$\phi_T = \frac{V}{A_m}\sqrt{\frac{k_r}{D_e}} = \delta\sqrt{\frac{k_r}{D_e}} \quad (11)$$

with D_e being the effective diffusivity of VOC in the catalyst material (m^2/s), estimated between 10^{-6} (random pore model) and 10^{-7} m^2/s (parallel pore model) [36]. The Thiele modulus has a maximum value in the order of 10^{-5} for the experiments of Table 3, which implies that the internal diffusion resistance is negligible. This was to be expected because the catalyst is applied as a very thin washcoat onto the fibers.

6. Transformation and discussion of the laboratory experimental results

6.1. The Arrhenius dependency of the reaction rate constant and temperature

Since exothermic reactions transform reactants into products with a lower level of potential energy, one might be tempted to conclude that these reactions will proceed spontaneously to their products. Were this true, no life would exist on earth, because the numerous carbon compounds that are present in and essential to all living organisms would spontaneously combust in the presence of oxygen to give carbon dioxide, a more stable carbon compound. The combustion of methane, for example, does not occur spontaneously, but requires an initiating energy in the form of a spark or a flame. The flaw in this reasoning is that it focuses only on the initial (reactants) and final (product) energy states of reactions. To understand why some reactions occur readily, almost spontaneously, whereas others are slow, even to the point of being unobservable, the intermediate stages of reactions need to be considered.

In order to transform the reactants into products, there must be a rearrangement of chemical bonds, which in the first instance, requires that some bonds are broken. The minimum level of energy needed to break these bonds, manifests itself as the activation energy (E). Only those molecule collisions which possess at least this minimum energy threshold can react to form products.

The source of the activation energy which enables a reaction to occur is often heat. At a higher temperature, more collisions will occur and a higher fraction of the collisions will possess the necessary activation energy for reaction. This temperature dependence of the reaction rate constant is expressed by the Arrhenius equation:

$$k_r = A \exp\left(-\frac{E}{RT}\right) \quad (12)$$

As stated before, catalytic combustion involves the use of a solid catalyst, which provides an alternative pathway between reactants and products and thus lowers the activation energy of the reaction. Because of the exponential relationship of k_r and E, small changes in activation energy will cause relatively large changes in reaction rate.

The oxidation also proceeds to a higher extent with increasing temperature. The activation energy, E, represents the energetics of reaction initiation on the surface of the catalyst. Provided that rapid and sufficient adsorption is possible [30], the breaking of the strongest bond within the initial (C)VOC or its eventual reaction intermediate can be considered as the probable rate-controlling process. These rate-factors are further included in the pre-exponential factor, A, a probabilistic factor which incorporates the additional requirements for the reaction to proceed at a given rate. The pre-exponential factor therefore also includes catalyst specific characteristics (e.g. type of catalyst, crystalline structure of the washcoat, number of active sites) and changes in the pre-exponential factor, A, have been previously correlated with deactivation of the catalyst [37].

6.2. Transformed experimental data: ln k_r versus 1/T and the activation energy

The reaction rate constants are calculated from the experimental destruction yields by Eq. (9) and plotted against $1/T$ (Figs. 11–13). The linear relationships obtained confirm the Arrhenius dependency.

The activation energy is calculated from the slope of the curves and results are given in Table 4. This table also compares the catalytic activation energies with the activation energies for the thermal (homogeneous) oxidation [38]. It is obvious that the use of the catalyst significantly decreases

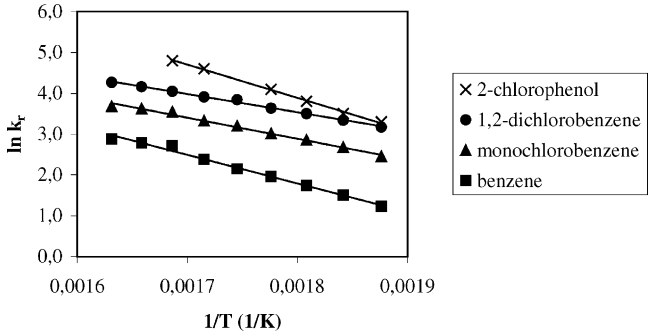

Fig. 11. Arrhenius dependency of reaction rate constant and temperature for benzene, monochlorobenzene, 1.2-dichlorobenzene and 2-chlorophenol.

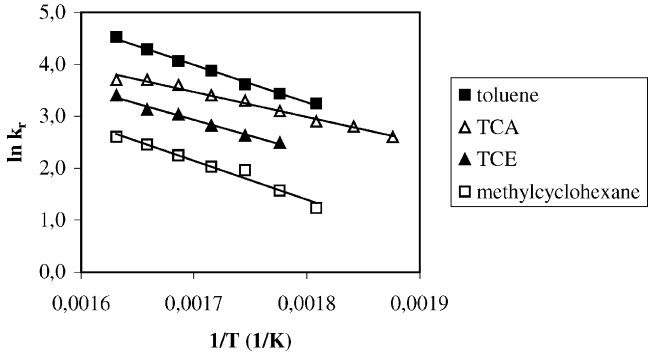

Fig. 12. Arrhenius dependency of reaction rate constant and temperature for toluene, methylcyclohexane, trichloroethylene and 1,1,1-trichloroethane.

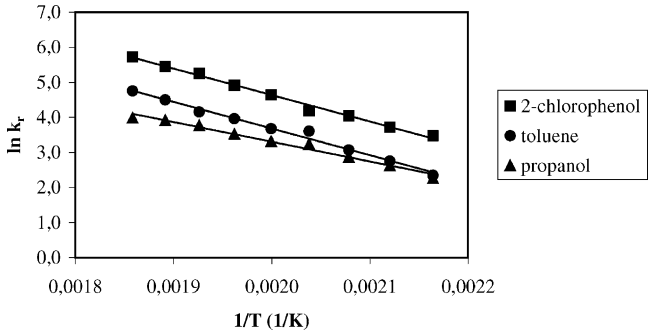

Fig. 13. Arrhenius dependency for Goretex REMEDIA®.

Table 4
Activation energy for the catalytic oxidation reaction

	Activation energy (kJ/mol)	
	Catalytic reaction	Thermal[a]
2-Chlorophenol	66.3	187.8
Benzene	58.4	189.9
Monochlorobenzene	42.9	188.1
1,2-Dichlorobenzene	37.3	187.1
Methylcyclohexane	62.4	189.1
Toluene	60.2	189.3
Trichloroethylene (TCE)	53.1	187.7
1,1,1-Trichloroethane (TCA)	40.4	187.6

[a] Calculated by the prediction method of [38].

Table 5
Activation energies for chlorinated benzenes calculated from literature data

	Activation energy (kJ/mol)	Author
Monochlorobenzene	47.0	Ide et al. [39]
1,2-Dichlorobenzene	40.8	Weber et al. [40]
1,2,3-Trichlorobenzene	30.4	Weber et al. [40]
1,2,4,5-Tetrachlorobenzene	23.7	Weber et al. [40]
Hexachlorobenzene	18.2	Weber et al. [40]
Hexachlorobenzene	18.0	Hagenmaier [41]

the activation energy in comparison with the homogeneous oxidation reaction.

The calculated values are between 37.3 and 58.4 kJ/mol for the benzenes and 66.3 kJ/mol for 2-chlorophenol. The activation energies are higher for the less or non-chlorinated benzenes. This observation can be confirmed by the results of Ide et al. [39], Weber et al. [40] and Hagenmaier [41], where destruction efficiencies for monochlorobenzene, 1,2,3-trichlorobenzene, 1,2,4,5-tetrachlorobenzene and hexachlorobenzene are reported. From these data, the activation energies are calculated and presented in Table 5.

The decrease in activation energy with increasing chlorination degree could be attributed to the lower energy of C–Cl bonds as compared to C–H bonds, respectively, 330 and 414 kJ/mol [42].

The activation energies of own and literature data are further discussed in Section 6.3.

The higher activation energy for TCE in comparison with TCA can be tentatively attributed to the lower energy of C–C bonds as compared to C=C bonds (347 kJ/mol versus 620 kJ/mol [26]). The activation energy for TCE over the V_2O_5–WO_3/TiO_2 also appears to be significantly lower than the value reported for Pt and PdO/γ-Al_2O_3 catalysts (81.2 and 142.3 kJ/mol, respectively) [37], which illustrates the strong affinity of vanadia for chlorine.

The higher activation energies for 2-chlorophenol, toluene and methylcyclohexane can be explained by the occurrence of highly stable reaction intermediates. The oxidation of the methyl-substituted ring structures includes the formation of an aldehyde or ketone as reaction intermediate, and in the oxidation pathway of 2-chlorophenol an aldehyde is formed. The further oxidation of this aldehyde or ketone includes the breaking of the very strong C=O bond (728 kJ/mol) which is most likely the rate-controlling step of the entire reaction pathway. The high stability of the reaction intermediate therefore determines the activation energies for these compounds, which are significantly higher than for the benzenes, TCE and TCA where the strongest bonds are, respectively, the C=C (620 kJ/mol) and C–H (415 kJ/mol) bonds.

6.3. Data treatment

6.3.1. Introduction

The experimental results of destruction efficiencies of the present work and of the literature can be transformed into

the reaction rate constants, accounting for the reaction time and possible mass transfer limitations [10]. The reaction rate constant, k_r, can thereafter be used to define the parameters of the Arrhenius dependency, i.e. the activation energy, E, and the pre-exponential factor, A.

When assessing literature data on catalytic combustion kinetics, extreme caution is needed since various authors use different approaches in their experiments and data treatment. There are:

(i) various forms of the rate expressions with reaction rates based on catalyst volume, catalyst external surface area, catalyst mass;

(ii) various ways of transforming kinetic constants using the space velocity (SV), the area velocity (AV) and/or the specific catalyst surface area (AP):

$$\text{SV} = \frac{\text{gas flow rate}}{\text{reactor volume}},$$

$$\text{at actual } \left(\frac{\text{m}^3/\text{h}}{\text{m}^3}\right) \text{ or standard } \left(\frac{\text{N m}^3/\text{h}}{\text{m}^3}\right) \text{ conditions}$$

$$\text{AV} = \frac{\text{gas flow rate}}{\text{catalyst surface area}},$$

$$\text{expressed as } \frac{\text{m}^3}{\text{m}^2\,\text{h}} \text{ or } \frac{\text{N m}^3}{\text{m}^2\,\text{h}}$$

$$\text{AP} = \frac{\text{catalyst surface area}}{\text{reactor volume}} \quad \left(\frac{\text{m}^2}{\text{m}^3}\right)$$

(iii) various ways of accounting for the catalyst coverage of the carrier material, i.e. in fractions or multiples of a monolayer coverage, including or omitting the possible catalytic effect of the carrier material itself;

(iv) different ways to include or omit influences of the carrier/catalyst geometry on the mass transfer resistance present in the system. The mass transfer resistance is overlooked by many authors, but will hereafter be shown to be important for some geometries.

As far as reaction kinetics are concerned, aspects (i)–(iv) can easily be accounted for and kinetic data transformed into the common s^{-1} kinetic constant or expressed as $m^3/(h\,m^2)$, thus independent of the catalytic set-up used. The aspects (i) and (iv) however are linked and some detailed calculations are necessary to enable the comparison of kinetic data obtained from different reactor geometries. The assessment of the mass transfer resistance in the catalytic fleeces used in the present research has been given in Section 5. A similar evaluation is shown in the following section for a honeycomb layout and for a fixed bed of catalytic pellets, both types of geometries commonly used in experiments. The comparison of kinetic data is thereafter illustrated for the oxidation of *o*-dichlorobenzene in the cases of a honeycomb set-up [39] and fixed pellet beds with different vanadia loadings [23,24,40].

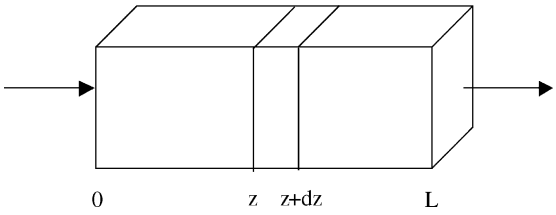

Fig. 14. Mass balance over an infinitesimal section of the reactor.

6.3.2. The effect of mass transfer resistances in the reaction rate expression

6.3.2.1. The honeycomb reactor of Ide et al. The catalytic reactor used by Ide et al. [39] for the oxidation of hydrocarbons consists of a honeycomb monolith (dimensions 150 mm × 150 mm × 800 mm, 26 × 26 cells) coated with a V_2O_5–WO_3/TiO_2 catalytic layer (thickness δ = 30 μm). From the given geometric surface area of the unit (582 m^2/m^3), the inner dimension of the square honeycomb cells (d_0) is calculated to be 4.8 mm.

A mass balance over a section of the reactor with length dz (Fig. 14) yields:

$$uS(C_{\text{HC}}(z) - C_{\text{HC}}(z + \text{d}z)) - \phi k_r C_{s,\text{HC}}\,\text{d}V = 0 \tag{13}$$

with u being the gas velocity in the reactor (m/s); S the cross-sectional area (m^2) = $d_0^2 \times 26 \times 26$; d$V$ the catalyst volume (m^3) = $4d_0 \times \delta \times 26 \times 26 \times \text{d}z$; C_{HC} the bulk concentration of VOC (mol/m^3); ϕ the effectiveness factor (the internal mass transfer resistance will be shown to be negligible: $\phi \approx 1$); k_r the intrinsic kinetic reaction constant (s^{-1}); $C_{s,\text{HC}}$ the concentration of VOC at the catalyst surface (mol/m^3).

A mass balance around the catalyst specifies that the rate of disappearance of VOC by reaction must equal the rate of transport of VOC to the catalyst surface:

$$\phi k_r C_{s,\text{HC}} V = k A_m (C_{\text{HC}} - C_{s,\text{HC}}) \tag{14}$$

with V/A_m = catalyst volume (m^3)/geometric catalyst surface (m^2) = d and k_m = external mass transfer coefficient (m/s).

The external mass transfer coefficient for the honeycomb configuration, k_m, can be obtained using the correlation for laminar flow in cylindrical ducts or channels [43] since the values of the Sherwood number in square channels approach the values for cylindrical ducts as the corners are rounded and filled with washcoat [44]:

$$Sh = 3.36\left(1 + 0.095\left(\frac{d_0}{L}\right) Re\,Sc\right)^{0.45} \tag{15}$$

with Sh being the Sherwood number (–); L the length of the honeycomb unit = 800 mm; Re the Reynolds number (–) based on the inner cell diameter d_0; Sc the Schmidt number (–) = $k_m d_0 / D_{\text{HC}}$; D_{HC} the diffusivity of VOC in air (m^2/s) (see Table 3).

A combination of Eqs. (13) and (14) yields the relationship between the surface concentration and the bulk concen-

Table 6
Evaluation of mass transfer resistance in the honeycomb reactor experiments of Ide et al. [39] (MCB: monochlorobenzene)

	η (%)	D_{HC} (m^2/s)	Sc (–)	Sh (–)	k_m (m/s)	k_0 (s^{-1})	k_r (s^{-1})	$(d_0/4k_m)/(1/\lambda) = C_{HC} - C_{s,HC}/C_{HC}$ (%)
Toluene	66	2.52×10^{-5}	1.89	3.98	2.07×10^{-2}	5.611	336.6	33
MCB	15	2.50×10^{-5}	1.91	3.99	2.06×10^{-2}	0.845	35.9	5

Experiments conducted at 300 °C, $Re = 422$.

tration:

$$C_s = \frac{1}{1 + \phi k_r \delta / k_m} C_b \tag{16}$$

By incorporating Eq. (16) in Eq. (13) and subsequent integration, the VOC conversion, η, is defined by

$$1 - \eta = \exp(-k_0 t) \quad \text{with} \quad \frac{1}{k_0} = \frac{d_0}{4\phi k_r \delta} + \frac{d_0}{4k_m} \tag{17}$$

The apparent reaction rate constant, k_0, is determined from the measured destruction efficiency, η, and the reaction time, t, with the use of Eq. (17). The intrinsic reaction rate constant k_r can then be calculated as follows:

$$k_r = \frac{\lambda d_0 k_m}{\delta\phi(4k_m - k_0 d_0)} \tag{18}$$

The external mass transfer can be assessed by calculating the contribution of mass transfer to the overall kinetic constant k_0 (Eq. (17)) and comparing the bulk concentration and the surface concentration of VOC:

$$\frac{C_b - C_s}{C_b} = \frac{1}{1 + k_m/\phi\delta k_r} = \frac{d_0/4k_m}{1/k_0} \tag{19}$$

Numerical results for the reactor of Ide et al. [39] are illustrated in Table 6 and demonstrate that mass transfer is not negligible in this reactor geometry. The omission of the mass transfer resistance can only be considered in the case of VOCs with very low destruction efficiencies, such as monochlorobenzene, where the kinetic constant is so low that the chemical reaction becomes the rate limiting step of the mechanism.

In the calculations of Table 6 the internal mass transfer resistance was omitted (effectiveness factor $\phi = 1$). Diffusion in the catalyst washcoat is not a rate-controlling step due to the very thin layer of catalyst applied to the honeycomb structure ($\delta = 30\,\mu m$). This can be verified using Eqs. (10) and (11). The effective diffusivity of the VOC in the catalyst pores is estimated between 10^{-6} (random pore model) and 10^{-7} m^2/s (parallel pore model) [36]. The Thiele modulus, ϕ_T, varies between 0.11 (monochlorobenzene) and 0.25 (toluene), which implies that the internal diffusion resistance is negligible ($0.96 < \phi < 0.99$).

6.3.2.2. The fixed pellet bed of Krishnamoorthy et al. Krishnamoorthy et al. [24] use a fixed bed of TiO_2-pellets coated with V_2O_5 and WO_3 for the oxidation of *o*-dichlorobenzene. Experiments were carried out with three pellet beds with varying vanadia content: 5.8, 3.6 and 0.8 wt.% V_2O_5 and a tungsten content of approximately 0.8 wt.% WO_3.

The fixed-bed reactor is best approached by a pseudo-homogeneous plug-flow model [36]. Reaction rate equations of Section 3 can therefore also be applied for this reactor system.

The mass transfer contributions will be evaluated for the experiments at 300 °C with the three different vanadia loadings. The fixed bed reactor contains 500 mg of pellets and the gas flow rate is 0.027 N m^3/h. At 300 °C, this results in a residence time of 32 ms.

From analyzing a large number of packed bed data, using the dispersed plug-flow model, Wakao and Kaguei [45] propose the following correlation for the determination of the external mass transfer coefficient, k_m:

$$Sh = \frac{k_m d_p}{D_{HC}} = 2 + 1.1\, Sc^{1/3}\, Re^{0.6} \tag{20}$$

with Sh being the Sherwood number (–); d_p the particle diameter (m) = 140 μm; D_{HC} the diffusivity of *o*-dichlorobenzene in air (m^2/s) Sc the Schmidt number (–) = 2.09; Re the Reynolds number (–), based on the particle diameter, is 0.044.

Application of this correlation yields a Sherwood number of 2.2 and a mass transfer coefficient, k_m, of 0.36 m/s.

Considering the composition and diameter of the pellet and the density of the catalyst material (3.357 g/cm^3 for V_2O_5, 3.84 g/cm^3 for TiO_2 and 7.16 g/cm^3 for WO_3), the thickness of the catalyst washcoat, δ, can be estimated at 1.7 μm (5.8 wt.%), 1.1 μm (3.6 wt.%) and 0.2 μm (0.8 wt.%), respectively.

The numerical evaluation is given in Table 7 and shows clearly that both the external and internal mass transfer resistances are negligible.

Table 7
Evaluation of mass transfer resistances in fixed bed reactor

	V_2O_5 (wt.%)		
	5.8	3.6	0.8
η (–)	0.77	0.41	0.24
k_0 (s^{-1})	46.3	16.6	8.6
δ/k_m (s)	4.9×10^{-6}	3.1×10^{-6}	6.4×10^{-7}
$(\delta/k_m)/(1/k_0)$ (%)	0.023	0.01	0.0005
ϕ_T (–)	0.005	0.002	0.0003
ϕ (–)	1	1	1

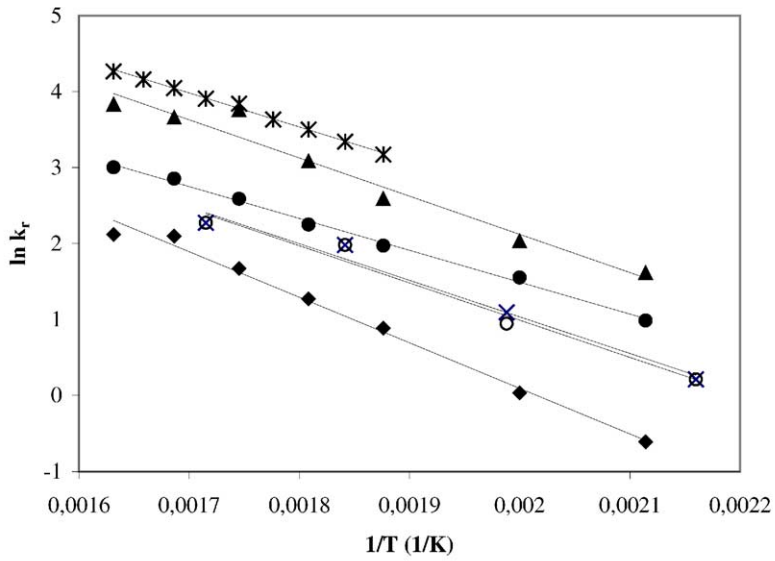

	Catalyst	Reference	Wt% V_2O_5	E (kJ/mol)	A (s^{-1})
✳	Metal fiber fleece	This work	3.2 – 3.5	37.3	110 415
▲	Fixed pellet bed	Krishnamoorthy et al. [24]	5.8	41.8	193 687
●	Fixed pellet bed	Krishnamoorthy et al. [24]	3.6	34.9	19 590
○	Fixed pellet bed	Weber et al. [40]	7.1	40.7	48 291
×	Fixed pellet bed	Weber et al. [40]	6.2	40.9	43 521
◆	Fixed pellet bed	Krishnamoorthy et al. [24]	0.8	42.2	30 761

Fig. 15. Overview of the Arrhenius relationship for the oxidation of *o*-dichlorobenzene for various vanadia catalysts.

6.3.3. The reaction rate constant (k_r) and the activation energy (E)

6.3.3.1. Illustration of results for o-dichlorobenzene (DCB). Fig. 15 illustrates the results obtained. Although k_r-values differ by an order of magnitude at a given value of $1/T$, the slopes of the graphs are fairly constant and define the activation energy which varies from 34.9 to 42.2 kJ/mol, with an average value of 39.6 kJ/mol.

Whereas the activation energy is a function of the combined characteristics of VOC and catalyst only, and hence a known parameter for the system, the kinetic constant itself and the pre-exponential factor are not only defined by the VOC under scrutiny, but also by the intrinsic properties of the catalyst such as matrix geometry, percentage of coverage of the carrier, total available surface area of the catalyst etc. This explains the inadequacy of the k_r-approach for a generalized design strategy.

6.3.3.2. Illustration of results for all VOCs (own experiments and literature). Similar k_r-results have been presented for own VOC-experiments in Section 5. Literature data were dealt within the same way and all data confirm the Arrhenius linearity of $\ln k_r$ versus $1/T$, thus defining the activation energy for each of the VOCs considered. The results are presented in Table 8.

In homogeneous VOC-oxidation reactions, the activation energy is correlated as a function of the molecular weight and type of VOC according to [38]:

$$E = a - b\,\mathrm{MW} \tag{21}$$

with a and b being slightly different constants for alkanes, aromatics, etc. The molecular weight is considered the key parameter in the kinetic energy of the molecule and in the efficiency of impact with the other reactant.

This simple E-versus-MW dependency does no longer hold for heterogeneous reactions. Certainly, the molecular weight still plays a key role as demonstrated in Fig. 16. The exponential function obtained for benzene, its chlorinated compounds and PCDD/F has a regression coefficient of 97.1%. The E(MW)-relationship for chlorinated phenols is still obvious although the regression coefficient is 89% only, due to the large deviation of 2-chlorophenol (MClPh).

The decreasing activation energy can still be explained by the increasing inherent energy of the large molecules (increasing the efficiency of impact with the catalyst), although other effects need to be accounted for, such as adsorption, VOC-volatility, steric hindrance, molecular polarization,

Table 8
Activation energy for VOCs

VOC	*E* (kJ/mol)	Reference
Benzene (Bz)	62.2	Ide et al. [39]
Benzene (Bz)	58.4	This work (metal fiber fleece)
Monochlorobenzene (MCB)	42.9	This work (metal fiber fleece)
Dichlorobenzene (DCB)	39.6	Average
Trichlorobenzene (TriCB)	30.4	Weber et al. [40]
Tetrachlorobenzene (TeCB)	23.7	Weber et al. [40]
Hexachlorobenzene (HxCB)	18.2	Weber et al. [40]
Hexachlorobenzene (HxCB)	18.0	Hagenmaier et al. [41]
PCDD	10.5	Liljelind et al. [51]
PCDF	13.1	Liljelind et al. [51]
PCDD/F	13.7	Fritsky et al. [52]
2-Chlorophenol (MClPh)	56.2	Ide et al. [39]
2-Chlorophenol (MClPh)	62.7	This work (Goretex Remedia)
2-Chlorophenol (MClPh)	66.3	This work (metal fiber fleece)
Dichlorophenol (DClPh)	27.7	Liljelind et al. [51]
Trichlorophenol (TriClPh)	19.1	Liljelind et al. [51]
Tetrachlorophenol (TeClPh)	16.3	Liljelind et al. [51]
Pentachlorophenol (PeClPh)	13.3	Liljelind et al. [51]
Toluene	63.6	This work (Goretex Remedia)
Toluene	60.2	This work (metal fiber fleece)
Methylcyclohexane	62.4	This work (metal fiber fleece)
Cyclohexane	38.5	This work (metal fiber fleece)
Ethylacetate	27.5	This work (metal fiber fleece)
Acetone	49.0	This work (metal fiber fleece)
1,1,1-Trichloroethane	40.4	This work (metal fiber fleece)
Trichloroethylene	53.1	This work (metal fiber fleece)
Propanol	46.9	This work (Goretex Remedia)
Propanol	42.6	This work (metal fiber fleece)
Butanol	44.0	This work (metal fiber fleece)

ionic strength, etc. Some of these effects also vary with the molecular weight, such as the enhanced adsorption of the larger molecules at the catalyst surface (as tentatively characterized by, e.g. the Freundlich constant, k_F, in Fig. 17), the volatility (quantified, e.g. by the normal boiling temperature or the vapor pressure) and the steric effects. They are therefore incorporated into the *E*-versus-MW dependency.

Other effects are more difficult to take into account. Various researchers have indicated that the energy of the strongest bond (E_b) within the VOC partly explained the difference in activation energy. Competing individual bonds within the investigated VOCs are C–Cl (330 kJ/mol), C=O (728 kJ/mol), C=C (620 kJ/mol), C–C (280 kJ/mol) and C–H (414 kJ/mol). This is a tentative explanation only, since it is unknown: (i) how the bonding energy will alter when the molecule is adsorbed and phenomena such as steric hindrance, molecule polarization and ionic strength are not accounted for; (ii) how the bonds are influenced by

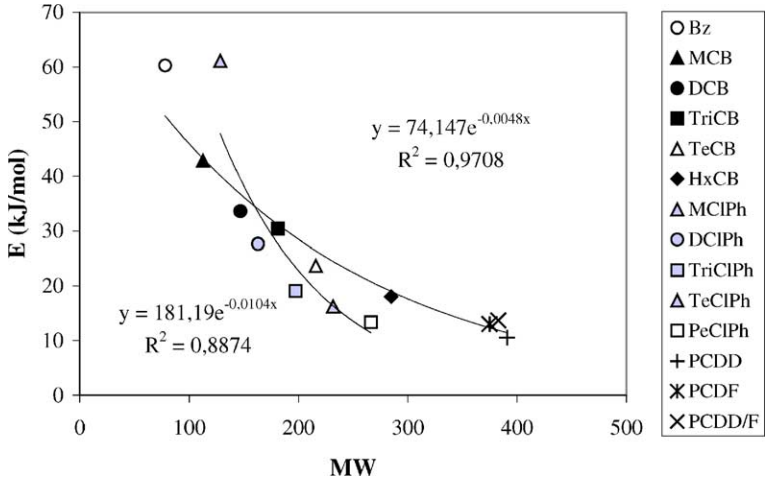

Fig. 16. Activation energy vs. molecular weight for various VOCs.

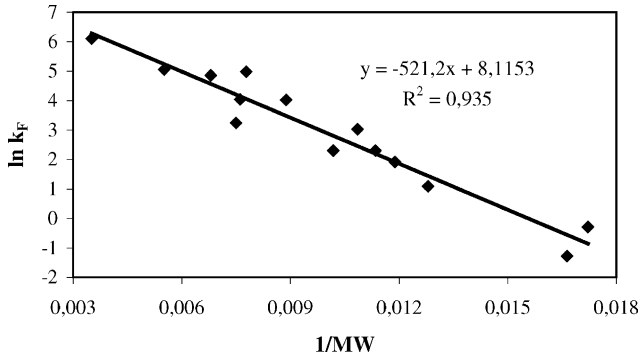

Fig. 17. Freundlich constant vs. molecular weight for various VOCs (Bz, MCB, DCB, TriCB, HxCB, toluene, MClPh, propanol, methylcyclohexane, cyclohexane, ethylacetate, 1,1,1-trichloroethane, trichloroethylene and acetone).

electronegative substituents (e.g. chlorine) being present. The effect of chlorine substitution in the benzene molecule is illustrated in Fig. 18. In terms of the cited bond energy, it appears that multiple chlorine substitution increasingly destabilizes the C=C bond, thus rendering the C–Cl bond dominant.

Although the presence of certain bonds can qualitatively explain differences in the activation energy, it is however impossible to present a generalized function of E versus E_b, since the dominant E_b is not clearly defined. It is therefore recommended to use the values of the experimentally defined activation energies and the derived E(MW)-correlations rather than assuming subjective relationships including the bond energy.

6.3.4. Transformation of the rate constant k_r into a system-independent constant K

As shown before, it is obvious that the kinetic constant is not only defined by the VOC under scrutiny, but also by the intrinsic properties of the catalyst itself. In order to generalize the kinetic expressions, catalyst properties are included by introducing the previously cited parameters AV ($m^3/(m^2\,h)$), AP (m^2/m^3) and SV (h^{-1}).

In doing so, a catalyst independent kinetic constant, K, is introduced:

$$K\left(\frac{m^3}{m^2\,h}\right) = \frac{3600k_r}{AP} = \frac{3600k_r AV}{SV} \quad (22)$$

The surface area of the catalyst is determined by the measured BET-value (m^2/g), the weight of the catalyst present (g) and the fractional coverage of the carrier, f_v.

Previous investigations have demonstrated that the catalyst is present as a monolayer and in full coverage provided the vanadia content is 0.145 wt.% V_2O_5/m^2 [46] or 13 μmol V^{5+}/m^2 [47]. Both values closely agree and their average value for full coverage is 0.1315 wt.% V_2O_5/m^2. The percentage of coverage is thus determined by the percentage of V_2O_5 present in the washcoat.

Application of these definitions to the different experimental investigations, determines the characteristic values of AV, AP and f_v, as illustrated in Table 9.

Results of k_r in s^{-1} can thus be transformed into K-values. Values for *o*-dichlorobenzene are again illustrated below for the various investigations, first (Fig. 19) for the experiments of Krishnamoorthy with three types of pellets only differing in V_2O_5-content (5.8, 3.6 and 0.8 wt.%), thereafter (Fig. 20) for all available data on *o*-dichlorobenzene.

The K-values for the results of Krishnamoorthy (Fig. 19) with the catalyst applied by a single technique on an identical carrier correlate very well ($R^2 = 0.93$). When introducing K-values for different carrier geometries, coating procedures and reaction circumstances, the correlation is less outspoken ($R^2 = 0.84$). Obtained K-values are however within the same order of magnitude for the various experiments with different types of vanadia catalysts and performed under varying circumstances. The remaining discrepancy is probably due to the uncertainty of the V_2O_5-crystal occurrence resulting from the largely different coating techniques applied [10]. The approach is however a meaningful step in the prediction of a design value for a reaction rate constant which is independent of the vanadia content and catalyst characteristics.

From the definition of the catalyst independent kinetic constant, K, in Eq. (22), it is obvious that this constant has the same temperature dependency as the kinetic constant k_r. The Arrhenius dependency can therefore also be expressed for K:

$$K\,(m^3/m^2\,h) = A^* \exp\left(-\frac{E}{RT}\right) \quad \text{with}$$

$$A^* = \frac{3600A}{AP} = \frac{3600AV}{SV} \quad (23)$$

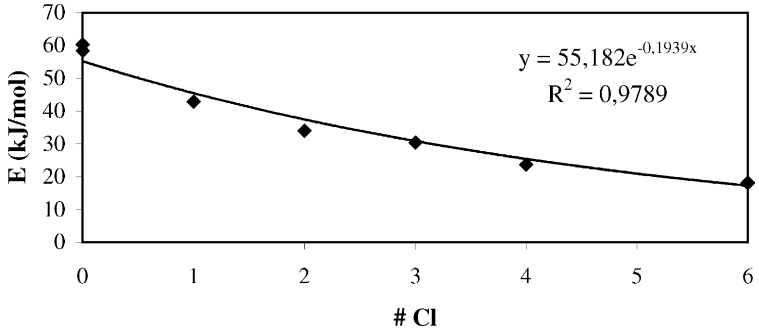

Fig. 18. Effect of chlorine substitution in benzene on the activation energy.

Table 9
Reactor characteristics for the experiments of Fig. 15

	Reference	AV ($m^3/(m^2\,h)$)	SV (h^{-1})	f_v (–)	AP (m^2/m^3)
*	This work	4.05×10^{-3}	139181	0.97–0.89	34365679
▲	Krishnamoorthy et al. [24]	2.84×10^{-3}	113341	0.52	39908803
●	Krishnamoorthy et al. [24]	5.10×10^{-3}	113341	0.32	22223725
○	Weber et al. [40]	3.80×10^{-4}	9777	0.90	25728947
×	Weber et al. [40]	4.35×10^{-4}	9777	0.79	22475862
◆	Krishnamoorthy et al. [24]	2.26×10^{-2}	113341	0.07	5015088

Note: AV and SV are given at a reference temperature of 300 °C.

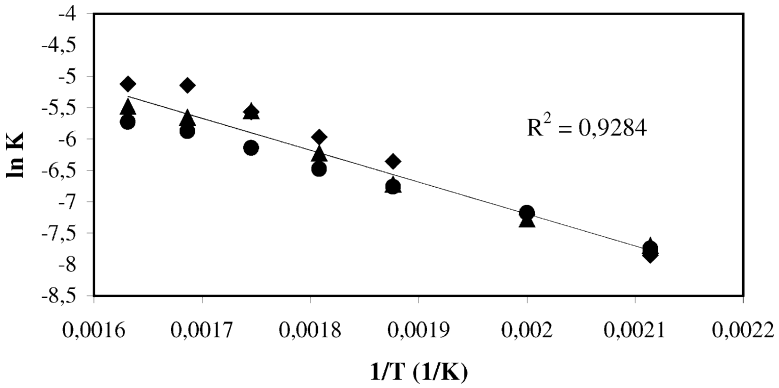

Fig. 19. Reaction rate constant (K), independent of catalyst coverage, for the experiments of Krishnamoorthy et al. [24] on *o*-dichlorobenzene.

with E being the activation energy, as summarized in Table 8, and A^* ($m^3/m^2\,h$) the pre-exponential factor, which is of course proportional to the pre-exponential factor for the calculation of k_r. The Arrhenius dependency of K is illustrated in Fig. 21 for various VOCs investigated in this work.

6.3.5. The pre-exponential factor A^*

6.3.5.1. Transformation into system-independency. As illustrated in Fig. 15, k_r and hence A-values are system-dependent and thus limited in design application to the specific catalyst layout under scrutiny. The characteristics of the catalyst reactor have been introduced through the definition of K (Eq. (22)), which is presented in Fig. 21 for own experiments. In doing so, general design data are obtained.

These exponential data again define:

(i) the activation energy, which is identical to the k_r-based values, the slope remaining unchanged through introducing the system-dependent but constant AP, AV and SV-values (Eqs. (22) and (23));
(ii) the system-independent pre-exponential factor A^*.

6.3.5.2. Correlating A^*. The validity of the Arrhenius equation encourages further probing into the concept of the energy barrier for reactions. Over the 100-year span

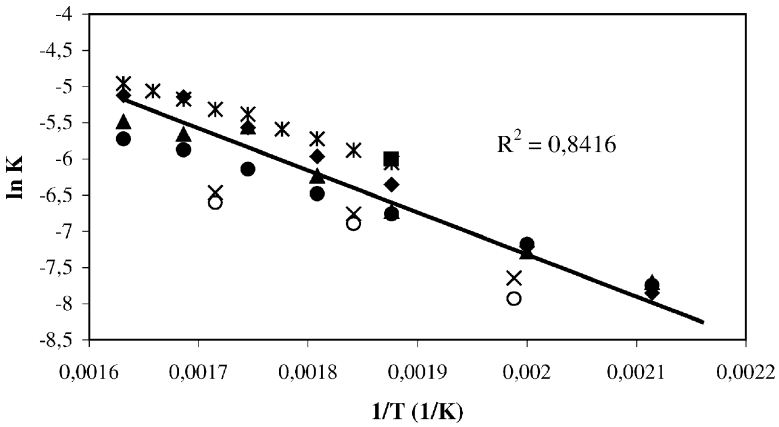

Fig. 20. K-values for *o*-dichlorobenzene for all available data.

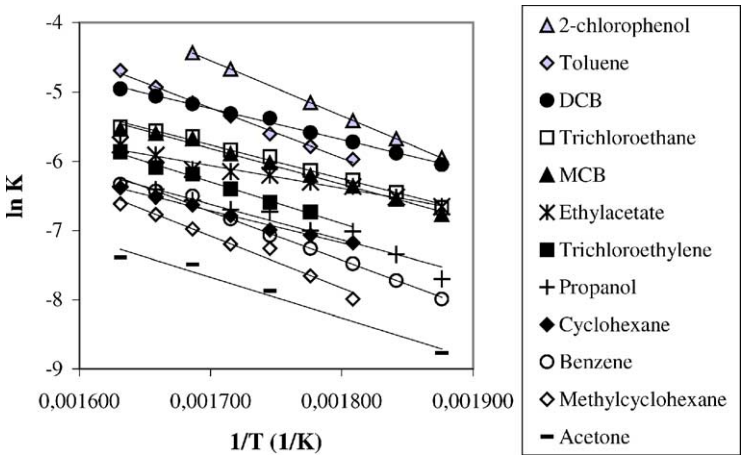

Fig. 21. Experimental results in terms of system-independent kinetic constant *K*.

of time since it was introduced, various efforts have been made to develop theories for reactions that could lead to predicting the value of rate constants. These include various collision theories, mostly for homogeneous reactions, and the transition-state, or activated-complex, theory for homogeneous and heterogeneous reactions [35, 48–50].

The transition-state theory provides a general concept involving the formation of an activated complex, the energy of which constitutes the barrier for forward reactions. It assumes an infinite number of active sites being available for the reactants. In this theory, reactants are assumed to be at equilibrium with an activated complex. The rate of reaction is expressed in terms of the number of such complexes crossing through the transition state. As a result of the theory, the rate constant of the reaction can be expressed as:

$$K \approx \mathrm{e}^{n} \frac{k_\mathrm{B} T}{h} \exp\left(\frac{\Delta S}{R}\right) \exp\left(-\frac{E}{RT}\right) = A^{*} \exp\left(-\frac{E}{RT}\right) \tag{24}$$

with k_B, h and R, respectively, being the Boltzmann, Planck and universal gas constants. The number of molecules participating in the reaction is given by parameter n. It is clear that A^{*} is a function of the entropy of activation (ΔS), and is therefore related to the difference in entropy between the activated state and the reactants.

For catalytic reactions, ΔS should be negative because of the immobility of the chemisorbed complex. Values of ΔS can be determined from the experimental linear form of $\ln K$ versus $1/T$. This has been performed for the data of the present research and corresponding literature data. In trying to correlate the obtained ΔS-values with relevant VOC and catalyst parameters, the best regression ($R^2 = 0.98$) was obtained in terms of the activation energy (Fig. 22) with

$$\Delta S\,(\mathrm{J/mol\,K}) = 2.25E - 337 \quad \text{with} \quad E \text{ in kJ/mol} \tag{25}$$

The existence of this dependency illustrates that for the studied VOC-catalyst systems, identical parameters determine the activation energy and the reaction rate.

It was previously demonstrated that the activation energy E is a combined function of mainly the molecular weight of the VOC, its adsorption characteristics and its volatility, which are moreover linearly dependent for the examined compounds. The concept of the activated complex relies on the same parameters of adsorption, volatility, molecule size and the proportionality with the activation energy is hence not surprising.

6.3.6. Overall comparison of predicted and experimental results

Having correlated the activation entropy, ΔS, in terms of the activation energy, E, and E in terms of the molecular weight, it is now possible to calculate K-values, transform them into k_r-values using the system-dependent characteristics (AP or AV and SV) and predict destruction efficiencies, taking into account the mass transfer limitations discussed previously.

The comparison of predicted and experimental data is illustrated in Fig. 23 for the group of chlorinated aromatic

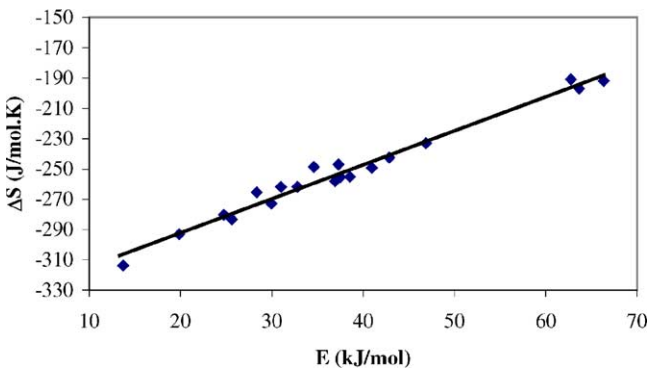

Fig. 22. Activation entropy vs. activation energy for investigated VOCs.

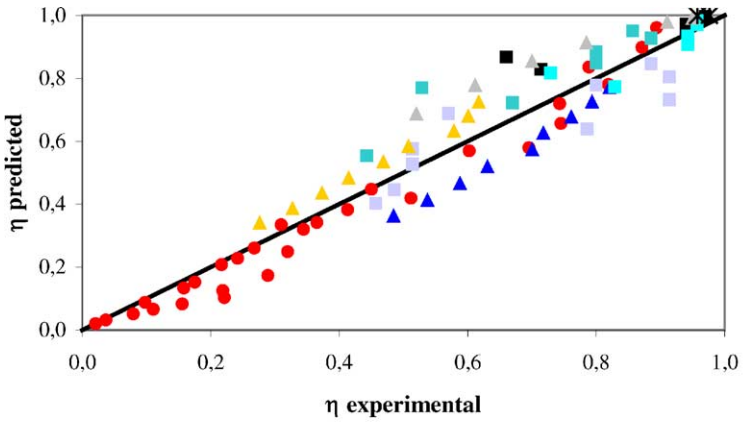

	Compound	Reference	Catalyst
▲	monochlorobenzene	This work	Metal fiber fleece
▲	1,2-dichlorobenzene	This work	Metal fiber fleece
◆	1,2-dichlorobenzene	Krishnamoorthy et al. [24]	Fixed pellet bed
■	1,2-dichlorobenzene	Weber et al. [40]	Fixed pellet bed
■	trichlorobenzene	Weber et al. [40]	Fixed pellet bed
■	tetrachlorobenzene	Weber et al. [40]	Fixed pellet bed
■	hexachlorobenzene	Weber et al. [40]	Fixed pellet bed
▲	o-chlorophenol	This work	Metal fiber fleece
✳	PCDD/F	Fritsky et al. [52]	Goretex Remedia

Fig. 23. Comparison of predicted and experimental destruction yields for chlorinated aromatics.

compounds. Although there remains a considerable scatter ($R^2 = 0.92$), the data points are centered around the diagonal of the graph, thus stressing the validity of the design approach.

7. Pilot-scale and full-scale results

Data were obtained at the 3000 N m^3/h pilot-scale of IVRO. The results are given in Table 10, which also includes results of Liljelind et al. [51] and full-scale data of Fritsky et al. [52]. These are the only literature reports where the various congeners are measured separately.

From the data it is clear that: (i) destruction efficiencies are normally excellent, with lower quoted values due to the use of the detection limit as exit concentration; (ii) the efficiencies increase with increasing operating temperature; (iii) the higher degree of chlorination does not markedly affect the destruction efficiency.

The Fritsky et al. [52] paper moreover reports an overall PCDD/F removal efficiency of 91.3% at an operating temperature of 194 °C.

The overall activation energy calculated from the results reported by Fritsky et al. [52] is 13.7 kJ/mol. The average activation energy calculated from the results of Liljelind et al. [51] is 13.1 kJ/mol for PCDD and 10.5 kJ/mol for PCDF. These data have already been included in the treatment of Section 6.3.

The catalytic destruction of PCDD/F being relatively new, literature data on separate PCDD/F destruction efficiencies are scarce. The final PCDD/F abatement (after carbon adsorption) is often combined with a vanadia catalyzed SCR

Table 10
PCDD/F catalytic destruction efficiencies (%)

	Own results IVRO (230 °C)	Liljelind et al. [51] (230 °C)	Fritsky et al. [52] (202 °C)
TCDD	99.10	92.0	94.44
PeCDD	98.86	97.0	95.45
HxCDD	97.30	95.0	90.63
HpCDD	96.72	92.0	92.82
OCDD	96.98	94.0	97.69
Average PCDD	97.8	94.0	95.2
TCDF	99.42	99.0	95.20
PeCDF	99.46	99.0	94.68
HxCDF	99.70	98.0	93.24
HpCDF	99.61	99.0	93.46
OCDF	99.61	97.0	98.84
Average PCDF	99.6	98.4	95.1

deNO$_x$ using NH$_3$. These SCR-data should be considered with extreme caution since the inlet PCDD/F-concentrations are extremely low due to the adsorption pretreatment thus producing rather inaccurate destruction data.

The author reviewed the data available from Flemish MSWIs (two units apply a separate catalytic destruction, whereas one plant combines entrained-phase adsorption and SCR-deNO$_x$). These data are given in Table 11. Results of the PCDD/F destruction efficiencies at MSWI 10 over the past 24 months have confirmed the excellent performance. Temperatures ranged from 209 to 230 °C and inlet PCDD/F concentrations varied between 0.3 and 6.7 ng TEQ/N m^3-dry at 11% O$_2$. The measured efficiencies ranged from 98.2 to 98.9%. A slight temperature dependency is found (adding 0.5% from 205 to 235 °C).

The full-scale separate PCDD/F abatement reactors score average efficiencies largely in excess of 95%.

The full-scale SCR-units should not be compared with the separate units, since SCR-deNO$_x$ normally requires temperatures around 300 °C, where PCDD/F de novo synthesis could occur thus reducing the destruction efficiency.

8. Final design recommendations for the catalytic oxidation of CVOC and PCDD/F

8.1. Preliminary observations

It should be remembered that most of the experimental investigations operate at conditions favoring the reaction to proceed at low to medium yields, since results at over 90% destruction efficiency will not allow the accurate determination of kinetic constants and activation energies. To produce useable results, experiments—including the work of this thesis—are carried out at: (i) high values of SV (h^{-1}), i.e. low contact times, as illustrated in Table 9 and (ii) low to medium reaction temperatures.

Literature data on industrial scale CVOC catalytic combustion however operate at slightly higher temperatures, longer contact times (SV between 10000 and 40000 h^{-1}) and possibly include mass transfer resistances when honeycomb geometries are used.

The Goretex REMEDIA® fleece reactor operates at temperatures between 220 and 250 °C, for SV-values between 10000 and 20000 h^{-1}. The mass transfer is negligible in the Goretex fleece.

Increasing the time of reaction, thus reducing the SV-values, is quite simply achieved by reducing the superficial gas velocity of the reactor, or increasing the thickness of the catalyst bed or fleece. The Bekaert fleece of 1 mm thickness, operating at 2 m^3/h (300 °C) yields a residence time of 12.4 ms (SV ≈ 290 000 h^{-1}). If operated at 2 or 10 mm thickness, the residence time is increased to 24.8 or 124 ms, respectively, with corresponding SV of 145 000 or 29 000 h^{-1}. The sintering of thicker fiber webs will then be needed and is technically easy to achieve.

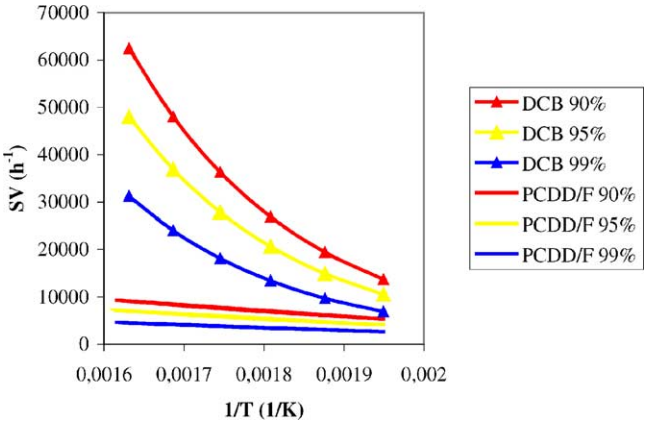

Fig. 24. Space velocity and temperature required for given destruction yields of *o*-dichlorobenzene (DCB) and PCDD/F with a metal fiber fleece (AP = 35 × 10^6 m^2/m^3).

8.2. Design values of a fleece reactor

In order to expand the experimental results to high destruction efficiencies and define the operating parameters to achieve these yields, calculations of Section 6 were repeated for the metal fiber fleece as used in our experimental work (AP = 35 × 10^6 m^2/m^3). Given temperatures and required conversion yields determine the acceptable contact time, expressed through the space velocity, SV (h^{-1}).

By way of example, these calculations have been made for *o*-dichlorobenzene (DCB) and PCDD/F, using experimental activation energies and entropies. Results are shown in Fig. 24 and stress the importance of operating at as a high temperature as is economically justified. The contact time can be read from the figure for a given temperature, a known catalyst configuration (AP) and a required conversion.

High destruction yields require lower SV-values than those used in the own and literature research, thus demand-

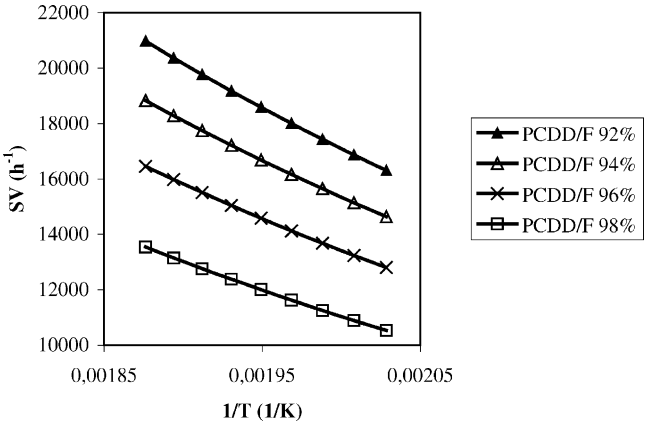

Fig. 25. Space velocity and temperature required for given destruction yields of PCDD/F with Goretex REMEDIA® (AP = 130 × 10^6 m^2/m^3).

Table 11
Review of full-scale destruction efficiencies

Reference	Operating temperature (°C)	Destruction efficiency (%)
Separate PCDD/F abatement		
MSWI 5-Flanders	210–240	98.3–99.4
MSWI 10-Flanders	209–240	93.3–98.9
Fritsky et al. [52]	202	95.1
Frings et al. [53]	190–240	99.0
Boos et al. [47]	280	97
Combined PCDD/F polishing and SCR-deNO$_x$		
Carlsson et al. [54]	325	80
MSWI 8-Flanders	214	95.4–98.3
Tartler et al. [55]	300	61.8
Ishida et al. [56]	200	83.3
Kamiyama et al. [57]	230	94.5

ing reduced superficial velocities and/or increased fleece thicknesses.

The calculation for the Goretex REMEDIA® fleece with average AP of $130 \times 10^6\ m^2/m^3$ and expected PCDD/F destruction efficiency between 92 and 98% is illustrated in Fig. 25. Predicted SV-values correspond with the cited industrial values, thus stressing the validity of the design approach suggested in this work.

9. Conclusions

Experimental investigations using a novel catalyst-coated sintered metal fleece are reported in this paper. Thin metal fibers are sintered (non woven) to fleece of various thickness, structure and porosity and with excellent dedusting capacities. The V_2O_5–WO_3/TiO_2 catalyst was applied by the spray coating technique, thus combining the catalytic destruction of (C)VOC and dedusting, if required.

Destruction efficiencies were measured with various (C)VOC in the temperature range of 260–340 °C. Literature data for oxidation reactions in fixed beds and honeycomb reactors are included in the assessment.

Mass transfer resistances are calculated and are generally negligible for fleece reactors and fixed pellet beds, but can be of importance for honeycomb monoliths.

The experimental investigations demonstrate: (i) that the conversion of the hydrocarbons is independent of the oxygen concentration, corresponding to a zero-order dependency of the reaction rate; (ii) that the conversion of the hydrocarbons is a first-order reaction in the (C)VOC; (iii) that the oxidation of the (C)VOC proceeds to a higher extent with increasing temperature, with multiple chlorine substitution enhancing the reactivity; (iv) that the reaction rate constant follows an Arrhenius-dependency.

The reaction rate constant k_r (s^{-1}) and the activation energy E (kJ/mol) are determined from the experimental results. The activation energy is related to the characteristics of the (C)VOC under scrutiny and correlated in terms of the molecular weight.

The k_r-values are system-dependent and hence limited in design application to the specific VOC-catalyst combination being studied. To achieve system-independency, k_r-values are transformed into an alternative kinetic constant K ($m^3/(m^2u)$) expressed per unit of catalyst surface and thus independent of the amount of catalyst present in the reactor. In doing so, largely different experimental data can be fitted in terms of this K-approach. Results are thereafter used to define the Arrhenius pre-exponential factor (A^*), itself expressed in terms of the activation entropy.

Destruction efficiencies for any given reactor set-up can be predicted from E- and A^*-correlations. The excellent comparison of predicted and measured destruction efficiencies for a group of chlorinated aromatics stresses the validity of the design approach.

Since laboratory-scale experiments using PCDD/F are impossible, pilot and full-scale tests of PCDD/F oxidation undertaken in Flemish MSWIs and obtained from literature are reported. From the data it is clear that: (i) destruction efficiencies are normally excellent; (ii) the efficiencies increase with increasing operating temperature; (iii) the higher degree of chlorination does not markedly affect the destruction efficiency.

Finally, all experimental findings are used in design recommendations for the catalytic oxidation of (C)VOC and PCDD/F. Predicted values of the acceptable space velocity correspond with the cited industrial values, thus stressing the validity of the design strategy and equations developed in the present chapter.

Appendix A. Literature review on (C)VOC oxidation over vanadia catalysts

Catalyst/operating conditions/tested (C)VOC	Results/comments
Mori, K., Inomata, M., 1984. J. Chem. Soc., Faraday Trans. I 80, 2655–2668	
Unsupported V_2O_5, V_2O_5/TiO_2 and V_2O_5/Al_2O_3	The catalyst activity was mainly determined by the number of surface V=O species
350–400 °C	The TiO_2supported catalyst showed the highest activity
Benzene	Zero-order kinetics in oxygen (for O_2-concentration >0.14 atm)
	Activation energies
	V_2O_5: 22 kcal/mol
	V_2O_5/TiO_2: 20–23 kcal/mol
	V_2O_5/Al_2O_3: 29–32 kcal/mol
Hagenmaier, H., 1989. VDI Berichte 730, 239–254	
Various metals and metal oxides	CVOC oxidation does not produce PCDD/F
Various CVOC, but mostly PCDD/F	Fly ash catalyzes the transition of congeners
	PCBs and PCDD/F can be catalytically oxidized (>99%) at 120–500 °C for residence times of 1–4 s
	Copper oxides yield very high conversions at >250 °C
	TCDF and hexachlorobenzene are virtually 100% destroyed at 500 °C
	SV should be $<1{,}000\,h^{-1}$
	The author specifies the different applications of catalytic CVOC destruction
Jin, L., Abraham, M.A., 1991. Ind. Eng. Chem. Res. 30, 89–95	
V_2O_5-powder catalyst (fixed bed reactor)	Small amounts of 1,2,4-trichlorobenzene were detected
288–343 °C	First-order kinetics in both DCB and oxygen concentration
1,4-Dichlorobenzene (DCB), 0.37 mol/l	Surface reaction proceeds more slowly than adsorption and is the rate limiting step in the oxidation mechanism
	Activation energy for DCB = 24.9 kJ/mol
Boos, R., Budin, R., Hartl, H., Stock, M., Wurst, F., 1992. Chemosphere 25 (3), 375–382	
V_2O_5–WO_3/TiO_2, honeycomb-type catalyst, 280 °C	η(PCDD/F) between 89 and 96%
PCDD/F	Combined deNO_x possible (injection of NH_3)
Frings, B., Marl, K., 1994. Umwelt-Special, K22	
V_2O_5–WO_3/TiO_2	First-order kinetics in VOC
Honeycomb	Reaction rate constants are given
2–4 wt.% V_2O_5	PCDD/F congeners are oxidized with equal efficiency
200–350 °C	η(PCDD/F) 94.9% at 210 °C and >98% above 325 °C
PCDD/F, perchloroethylene, dichlorobenzene	Simultaneous deNO_x: η >70% and function of operating temperature
Ide, Y., Kashiwabara, K., Okada, K., Mori, S., Hara, M., 1996. Chemosphere 32, 189–198	
V_2O_5–WO_3/TiO_2 (SCR catalyst)	η increases with increasing temperature or decreasing AV
Honeycomb catalyst	First-order kinetics in VOC
210–260 °C	NO_x reduction possible with same catalyst
Bench scale test equipment	Design equations for deNO_x included
Field test equipment used on MSW flue gas	η(PCDD/F) is approx. 90%
Benzene, toluene, polychlorobenzenes (PCBz), polychlorophenols (PCPh), PCDD/F	Addition of NH_3 does not affect PCDD/F-decomposition
	η(PCBz) less than 30%
	η(PCPh) >85%
	Activation energy of PCPh is lower than that of PCBz

Appendix A (*Continued*)

Jones, J., Ross, J.R.H., 1997. Catalysis Today 35, 97–105	
V_2O_5 (4 wt.%) supported on TiO_2, ZrO_2, SiO_2, Al_2O_3 and La_2O_3	100% conversion at temperatures >300 °C
Pellets in fixed bed	CO_2, H_2O and HCl are the only reaction products detected
140–500 °C	Catalyst is stable in presence of HCl
Ethylchloride, monochlorobenzene	Addition of WO_3 improves the resistance to SO_2 poisoning, but has no significant effect on catalytic behavior
Oxidation reactions in presence of NO and NH_3	$deNO_x$ data are also included
Krishnamoorthy, S., Baker, J.P., Amiridis, M.D., 1998. Catalysis Today 40, 39–46	
V_2O_5/TiO_2 catalyst with different V_2O_5 loadings (0.8, 3.6 and 5.8 wt.%) and different additives (none, WO_3, MoO_3 and ZnO)	DCB selected because of structural similarity to PCDD/F
Fixed bed reactor with pellets (80–120 mesh)	No intraparticle diffusional limitations
100–500 °C	TiO_2 support also exhibits some activity for DCB oxidation
1,2-Dichlorobenzene (DCB)	First-order kinetics in DCB, zero order in O_2
	The addition of WO_3, MoO_3 or ZnO has a promoting effect on SCR-activity (reduction of NO_x in the presence of NH_3), but does not alter the DCB-oxidation activity
	Addition of NH_3 enhances oxidation of DCB
	η increases with temperature and V_2O_5 loading
	η > 80% at T > 330 °C and 5.8 wt.% V_2O_5
	Activation energy: 30–37 kJ/mol
	CO and CO_2 are the only carbon-containing reaction products
	No catalyst deactivation after 100 h of operation at 723 K
Weber, R., Sakurai, T., Hagenmaier, H., 1999. Applied Catalysis B: Environmental 20, 249–256	
V_2O_5–WO_3/TiO_2	h(PAH) > 95% and h(PCDD/F) > 98%
Honeycomb-type catalyst, crushed and used as fixed bed	h(PCBz) = 99% above 300 °C and 50% at 200 °C
Average composition: 80 wt.% TiO_2, 6–7 wt.% V_2O_5 and 5.5–6 wt.% WO_3	At temperatures below 200 °C, removal is mainly caused by adsorption on the catalyst
SV = 5000 h^{-1} (cf. SCR-catalyst in MSWIs)	Higher chlorinated PCDD/F have lower oxidation rates
150–310 °C	Oxidation rate of PCBz increases with chlorination degree
PCDD/F, polychlorobenzenes (PCBz), polyaromatic hydrocarbons (PAH)	An explanation for the high adsorption affinity of PAHs and PCDD/F on the catalyst is given
	Destruction results are explained by competing effects of redox potential and volatility
Donghoon, S., Sangmin, C., Jeong-Eun, O., Yoon-Seok, C., 1999. Environ. Sci. Technol. 33, 2657–2666	
V_2O_5–WO_3/TiO_2	Results of Frings et al. (1994) and Ide et al. (1996) are used to develop an empirical correlation for η, applicable at temperatures above 175 °C
PCDD/F	
Krishnamoorthy, S., Rivas, J.A., Amiridis, M.D., 2000. J. Catal. 193, 264–272	
Cr_2O_3, V_2O_5, MoO_3, Fe_2O_3 and Co_3O_4 supported on TiO_2 and Al_2O_3	Cr_2O_3- and V_2O_5-based catalysts have highest activity
Metal oxide loadings (4.5–9 wt.%) are such that all catalysts have same amount of metal on molar basis (approx. 6×10^{-4} mol/g)	TiO_2-supported systems are more active than Al_2O_3-systems

Appendix A (*Continued*)

Fixed bed reactor with pellets (80–120 mesh)	TiO_2 also exhibits some oxidation activity
SV = 25,000 h^{-1}	Partial oxidation products (acetates, formeates, maleates and phenolates) are detected on the catalyst surface
1,2-Dichlorobenzene (DCB), 600 ppmv	Surface oxygen is involved in the oxidation reaction
	Oxidation reaction operates via similar mechanism for all investigated catalyst systems
Weber, R., Plinke, M., Xu, Z., 2000. Organohalogen Compounds 45, 427–430 and Weber, R., Plincke, M., Xu, Z., Wilken, M., 2001. Applied Catalysis B: Environmental 31, 195–207	
V_2O_5–WO_3/TiO_2 on PTFE-filter medium	Blank tests showed neither destruction nor adsorption on uncoated PTFE-filter
Commercially available as REMEDIA™ D/F by W.L. Gore & Associates, Inc.	PCDD/F destruction efficiency in excess of 99% with inlet concentrations of up to 100,000 ng/N m^3 (PCDD/F-values in MWIs are typically 200–4000 ng/N m^3)
8% V, <8% W	Adsorption on catalytic filter is important for $T < 200\,^{\circ}C$
SV = 25,000 h^{-1}, corresponds to typical filter velocity for industrial cloth filters (1 m/min)	PCDD were removed with slightly higher efficiency than PCDF
Laboratory set-up (200 °C)	Destruction kinetics of PCDD/F decrease with increasing chlorination degree
Field tests in MSWIs (185–220 °C)	η(benzo[a]pyrene) > 99.9%, η(pyrene) = 99.8%, η(naphthalene) = 75%
PCDD/F, non-chlorinated PAHs	No catalyst deactivation after 2 years of operation in MSWI, catalyst promises the same lifetime expectation as the filter bag material (5 years)
Plinke, M., Fritsky, K., Ganatra, C.P., Wilken, M., Gass, H., Weber, R., Mogami, Y., 2000. Organohalogen Compounds 45, 452–455	
REMEDIA™ D/F catalytic filter system by W.L. Gore & Associates, Inc.	η(PCDD/F) > 99%
PCDD/F-removal data of plants operating with the filter (incinerators, crematoria and steel mills)	PCDD/F are destroyed and not just adsorbed on catalyst or dust cake
180–250 °C, filter velocity 1 m/min	In 8 of the 14 examined plants, dust emissions cannot exceed 1 mg/N m^3 to comply to the 0.1 ngTEQ/N m^3-norm
	Seven plants operating with the filter for up to 3 years have PCDD/F-emissions below 0.1 ngTEQ/N m^3
Xu, Z., Fritsky, K., Graham, J., Dellinger, B., 2000. Organohalogen Compounds 45, 419–422	
Lab-scale: V_2O_5/TiO_2-powder catalyst, 230 °C, PCDD/F (<100 ppb)	Lab-scale: η(PCDD/F) > 99.6%
Results of REMEDIA™ D/F catalytic filter system on medical waste incinerator are also reported (194–204 °C)	Only inorganic reaction products were formed
	No adsorbed TCDD was found on the catalyst
	Medical waste incinerator: PCDD/F-emissions are reduced from 2.57 to approx. 0.05 ng TEQ/N m^3@11% O_2
Fritsky, K.J., Kumm, J.H., Wilken, M., 2001. J. Air & Waste Manage. Assoc. 51, 1642–1649	
REMEDIA™ D/F catalytic filter system by W.L. Gore & Associates, Inc.	The total PCDD/F removal efficiency is 98.4%, composed of a gas-phase destruction efficiency of 97.7% and a solid phase removal efficiency of 99.9%
Results of medical waste incinerator (136.4 tons per day, =200 °C)	the clean gas PCDD/F concentration is $\ll$0.1 ng TEQ/N m^3-dry at 11% O_2

Appendix A (*Continued*)

PCDD/F inlet concentration: 1.77 ng TEQ/N m^3 in gas phase and 0.80 ng TEQ/N m^3 in solid phase	The particulate matter removal efficiency is 99.95% Life expectancy of the filter system is 5 operating years
Liljelind, P., Unsworth, J., Maaskant, O., Marklund, S., 2001. Chemosphere 42, 615–623	
TiO_2–V_2O_5 extrudate (commercial catalyst for Shell Denox System) 100–250 °C Operated at SV 8,000 and 40,000 h^{-1} PCDD/F, PCBs, PAHs, polychlorobenzenes (PCBz), polychlorophenols (PCPh)	At low temperatures (100 °C) PCDD/F-removal is mainly caused by adsorption on catalyst At 230 °C all removal is by destruction η increases with temperature η(PCDD/F): >92.5% and η(PCBs): 46–76% η(PAHs): 75–98% η(PCBz): 33%, no adsorption observed η(PCPh): 98%, no adsorption observed Chloro-homologue profiles remain unaffected PCPhs have higher activation energies than PAHs and PCDD/F
Weber, R., Sakurai, T., 2001. Applied Catalysis B: Environmental 34, 113–127	
V_2O_5–WO_3/TiO_2 Honeycomb-type catalyst, crushed and used as fixed bed Average composition: 78.2 wt.% TiO_2, 7.1 wt.% V_2O_5 and 5.9 wt.% WO_3 SV = 5000 h^{-1} (cf. SCR-catalyst in MSWIs) 150–300 °C PCB	Adsorption of PCB on catalyst (71% of PCB-feed at 150 °C, 12% at 210 °C and 0.05% at 250 °C) η(PCB) > 99% for T > 200 °C PCB destruction rate increases with decreasing chlorination degree PCB removal efficiency decreases with decreasing chlorination degree PCDF are formed during decomposition of PCB, but are also oxidized on the catalyst T > 250 °C: no PCDF were detected No PCDD, nor any other by-products, were detected

References

[1] K. Everaert, J. Baeyens, C. Creemers, A comparative study of abatement techniques for volatile organic compounds, in: Proceedings of the CHISA International Conference, vol. 2, Prague, August 25–29, 2002, pp. 23–25.

[2] K. Everaert, J. Baeyens, J. Degrève, Removal of PCDD/F from incinerator flue gases by entrained-phase adsorption, J. Air Waste Manage. Assoc. 52 (2002) 1378–1388.

[3] K. Everaert, J. Baeyens, Formation and emission of dioxins in large scale thermal processes, Chemosphere 46 (2002) 439–448.

[4] K. Everaert, J. Baeyens, Correlation of PCDD/F emissions with operating parameters of municipal solid waste incinerators, J. Air Waste Manage. Assoc. 51 (2001) 718–724.

[5] H. Huang, Formation mechanisms of polychlorinated dibenzo-*p*-dioxins and dibenzofurans in combustion processes, Ph.D. Thesis, Vrije Universiteit, Brussel, 1999.

[6] E.J. Sare, J.M. Lavanish, US Patent 4 065 543 (1977).

[7] T.L. Wolford, US Patent 4 423 024 (1981).

[8] A.D. Harley, US Patent 4 816 609 (1989).

[9] B. Mendyka, J.D. Rutkowski, Study of the effect of hydrochloric acid on the activity of platinum catalysts, Environ. Prot. Eng. 10 (1984) 5–20.

[10] K. Everaert, The preventive reduction and "end-of-pipe" removal of VOC and PCDD/F from flue gas, Ph.D. Thesis, University of Leuven. ISBN 90-5682-423-6, 2003.

[11] M.P. Manning, Fluid bed catalytic oxidation: an underdeveloped hazardous waste disposal technology, J. Hazard. Waste 1 (1984) 41–65.

[12] S.L. Hung, L.D. Pfefferle, Methyl chloride and methylene chloride incineration in a catalytically stabilized thermal combustor, Environ. Sci. Technol. 23 (1989) 1085–1091.

[13] P. Subbanna, H. Greene, F. Desai, Catalytic oxidation of polychlorinated biphenyls in a monolithic reactor system, Environ. Sci. Technol. 22 (1988) 557–561.

[14] S. Imamura, H. Tarumoto, S. Ishida, Decomposition of 1,2-dichloroethane, Ind. Eng. Res. 28 (1989) 1449–1452.

[15] H.G. Stenger Jr., G.E. Buzan, J.M. Berty, Chlorine capture by catalyst-sorbents for the oxidation of air pollutants, Appl. Catal. B 2 (1993) 117.

[16] S.C. Petrosius, R.S. Drago, V. Young, G.C. Grunewald, Low-temperature decomposition of some halogenated hydrocarbons using metal oxide/porous carbon catalysts, J. Am. Chem. Soc. 115 (1993) 6131.

[17] J. Jones, J.R.H. Ross, The development of supported vanadia catalysts for the combined catalytic removal of the oxides of nitrogen and of chlorinated hydrocarbons from flue gases, Catal. Today 35 (1997) 97–105.

[18] S. Krishnamoorthy, J.A. Rivas, M.D. Amiridis, Catalytic oxidation of 1,2-dichlorobenzene over supported transition metal oxides, J. Catal. 193 (2000) 264–272.

[19] A. Beretta, E. Tronconi, G. Groppi, P. Forzatti, Monolithic catalysts for the selective reduction of NO_x with NH_3 from stationary

sources, in: A. Cybulski, J.A. Moulijn (Eds.), Structured Catalysts and Reactors, Marcel Dekker, New York, 1998, pp. 121–148.
[20] K. Everaert, N. Viggria, J. Baeyens, Hot gas media filtration by ceramic and sintered steel fiber candles, in: Proceedings of the Sixth World Congress of Chemical Engineering, Melbourne, September 23–27, 2001, CD-ROM.
[21] A. Aranzabal, R. Lopez-Fonseca, J.A. Gonzalez-Marcos, J.I. Alvarez, M.A. Gutierez-Ortiz, J.R. Gonzalez-Velasco, Controlling effluent composition in the chlorinated VOC catalytic oxidation, in: Proceedings of the International Congress CHISA, session I 4.4, Prague, August 27–31, 2000, pp. 1–11.
[22] R.E. Hayes, S.T. Kolaczkowski, Introduction to Catalytic Combustion, Gordon and Breach, 1997, p. 144.
[23] R. Weber, M. Plinke, Z. Xu, M. Wilken, Destruction efficiency of catalytic filters for polychlorinated dibenzo-*p*-dioxin and dibenzofurans in laboratory test and field operation—insight into destruction and adsorption behavior of semivolatile compounds, Appl. Catal. B 31 (2001) 195–207.
[24] S. Krishnamoorthy, J.P. Baker, M.D. Amiridis, Catalytic oxidation of 1,2-dichlorobenzene over V_2O_5/TiO_2-based catalysts, Catal. Today 40 (1998) 39–46.
[25] R. Weber, T. Sakurai, Low temperature decomposition of PCB by TiO_2-based V_2O_5/WO_3 catalyst: evaluation of the relevance of PCDF formation and insights into the first step of oxidative destruction of chlorinated aromatics, Appl. Catal. B 34 (2001) 113–127.
[26] R. Chang, Chemistry, 5th ed., McGraw-Hill, New York, 1994, p. 360.
[27] K.R. Westerterp, L. Van de Beld, M.C. Van der Ven, A kinetic study of the complete oxidation of ethene, propane and their mixtures on a Pd/Al_2O_3 catalyst, Chem. Eng. Process. 34 (1995) 469–478.
[28] G.I. Golodets, Heterogeneous Catalytic Reactions Involving Molecular Oxygen, 3rd ed., Elsevier, Amsterdam, 1983, pp. 388, 499, 793.
[29] H. Windawi, M. Wyat, Catalytic destruction of halogenated volatile organic compounds, Platinum Met. Rev. 37 (1993) 186–193.
[30] J.R. Gonzalez-Velasco, A. Aranzabal, J.I. Gutierrez-Ortiz, R. Lopez-Fonseca, M.A. Gutierrez-Ortiz, Activity and product distribution of alumina supported platinum and palladium catalysts in the gas-phase oxidative decomposition of chlorinated hydrocarbons, Appl. Catal. B 19 (1998) 189–197.
[31] D. Kunii, O. Levenspiel, Fluidization Engineering, Wiley, New York, 1969, pp. 196–197.
[32] R.E. Hayes, S.T. Kolaczkowski, Introduction to Catalytic Combustion, Gordon and Breach, 1997, pp. 228–229.
[33] R. Aris, On shape factors for irregular particles. I. The steady state problem. Diffusion and reaction, Chem. Eng. Sci. 6 (1957) 262.
[34] A. Wheeler, in: W.G. Frankenburg, V.I. Komarewsky, E.K. Rideal (Eds.), Advances in Catalysis, vol. III, Academic Press, New York, 1951.
[35] J.M. Smith, Chemical Engineering Kinetics, Reaction and Diffusion within Porous Catalysts, 2nd ed., McGraw-Hill, New York, 1970, Chapter 11, pp. 430–432.
[36] R.E. Hayes, S.T. Kolaczkowski, Introduction to Catalytic Combustion, Gordon and Breach, 1997, pp. 246–248.
[37] H. Shaw, Y. Wang, Y. Tia-Chang, A.E. Cerkanowicz, Emerging Technologies in Hazardous Waste Management III, Catalytic Oxidation of Trichloroethylene and Methylene Chloride, American Chemical Society, 1993, Chapter 17, pp. 358–379.
[38] C.D. Cooper, F.C. Alley, Air Pollution Control, VOC Incinerators, Waveland Press Inc., Illinois, Chapter 4, 1994.
[39] Y. Ide, K. Kashiwabara, K. Okada, S. Mori, M. Hara, Catalytic decomposition of dioxin from MSW incinerator flue gas, Chemosphere 32 (1996) 189–198.
[40] R. Weber, T. Sakurai, H. Hagenmaier, Low temperature decomposition of PCDD/PCDF, chlorobenzenes and PAHs by TiO_2-based V_2O_5–WO_3 catalysts, Appl. Catal. B 20 (1999) 249–256.
[41] H. Hagenmaier, Katalytische Oxidation halogenierter Kohlenwasserstoffe unter besonderer Berücksichtigung des Dioxinproblems, VDI Berichte 730 (1989) 239–254.
[42] CRC Handbook of Chemistry and Physics, 81st ed., CRC Press, Boca Raton, 2000.
[43] W.M. Kays, A.L. London, Compact Heat Exchangers, 2nd ed., McGraw-Hill, New York, 1964.
[44] R.K. Shah, A.L. London, Laminar Flow Forced Convection in Ducts, Academic Press, New York, 1978.
[45] N. Wakao, S. Kaguei, Heat and Mass Transfer in Packed Beds, Gordon and Breach, London, 1982.
[46] G.C. Bond, K. Bruckman, Selective oxidation of o-xylene by monolayer V_2O_5–TiO_2 catalysts, Faraday Disc., Chem. Soc. 72 (1981) 235–246.
[47] R. Boos, R. Budin, H. Hartl, M. Stock, F. Wurst, PCDD and PCDF destruction by a SCR-unit in a municipal waste incinerator, Chemosphere 25 (1992) 375.
[48] J.C. Jungers, J.C. Balaceanu, F. Coussemant, F. Eschard, A. Giraud, M. Hellin, P. Leprince, G.E. Limido, Cinétique Chimique Appliquée, Société des Edtions Technip, Paris, 1958, pp. 246–250, and 278–282.
[49] H.I. Rase, Fixed-Bed Reactor Design & Diagnostics, Butterworths, London, 1990, pp. 42–48.
[50] P.C. Houston, Chemical Kinetics & Reactor Dynamics, McGraw-Hill, New York, 2001, pp. 102–111.
[51] P. Liljelind, J. Unsworth, O. Maaskant, S. Marklund, Removal of dioxins and related aromatic hydrocarbons from flue gas streams by adsorption and catalytic destruction, Chemosphere 42 (2001) 615–623.
[52] K.J. Fritsky, J.H. Kumm, M. Wilken, Combined PCDD/F destruction and particulate control in a baghouse: experience with a catalytic filter system at a medical waste incineration plant, J. Air Waste Manage. Assoc. 51 (2001) 1642.
[53] B. Frings, K. Marl, Katalytische Dioxin-Minderung. Umwelt-Special, 1994, pp. K22–K26.
[54] K.B. Carlsson, Dioxin removal in "energy from waste" plants—comparison of air pollution control methods, Organohalogen Compd. 18 (1989) 1731.
[55] M. Tartler, M. Vermeulen, T. Van Winden, Dioxin reduction in domestic waste incineration plant—the AVA Nijmegen plant as an example, Organohalogen Compd. 27 (1996) 68.
[56] M. Ishida, R. Shiji, P. Nie, N. Nakamura, S.-I. Sakai, Full-scale plant study of low temperature thermal dechlorination of PCDD/F, Organohalogen Compd. 27 (1996) 147.
[57] E. Kamiyama, K. Hamabe, M. Kondo, Behaviour of PCDDs, PCDFs and coplanar PCBs in MSW incinerators, Organohalogen Compd. 19 (1994) 401.